

# Crystallization of Groundmass Spinel in Kimberlite

P. L. ROEDER<sup>1</sup>\* AND D. J. SCHULZE<sup>2</sup>

<sup>1</sup>DEPARTMENT OF GEOLOGICAL SCIENCES, QUEEN'S UNIVERSITY, KINGSTON, ONTARIO K7L 3N6, CANADA

<sup>2</sup>DEPARTMENT OF GEOLOGY, UNIVERSITY OF TORONTO, ERINDALE COLLEGE, MISSISSAUGA, ONTARIO L5L 1C6, CANADA

RECEIVED AUGUST 8, 2007; ACCEPTED JUNE 17, 2008  
ADVANCE ACCESS PUBLICATION JULY 19, 2008

Groundmass spinel grains in 46 kimberlite and related rocks have been analyzed and compared. The majority of the spinel analyses are classified as high-chromium chromite (Chr) and magnesio-ulvöspinel–magnetite (Mum) and represent two significant stages of spinel growth. There are also a significant number of spinel grains that are classified as xenocryst spinel (Xen), pleonaste spinel (Ple) and magnetite (Mag). Eight different spinel zoning trends are identified. The majority of the Chr spinel grains are interpreted as a primary phase that crystallized as small octahedra from kimberlite magma on the journey from the upper mantle to the final resting place in the upper crust. Three zoning trends lead directly away from primary chromite. The major zoning trend, Trend 1, is from chromite to magnesio-ulvöspinel–magnetite. This zoning trend is unique to spinel in kimberlite, carbonatites and lamprophyres. We suggest that this somewhat oxidizing, and more magnesian, trend was influenced by the high carbonate content of Group I kimberlites and the rapid crystallization of the minerals during the evolution of volatiles. The zoning Trend 2 involves increasing titanium and ferric iron as a function of increasing  $Fe^{2+}/(Fe^{2+} + Mg)$ . This trend is similar to the zoning of spinel in basalt and is thought to be due to co-crystallization of magnesium- and aluminum-rich silicate minerals such as olivine and phlogopite in kimberlites, or pyroxene and plagioclase in basalt. Zoning Trend 3 in kimberlite leads away from primary chromite and towards an aluminous pleonaste (Ple) spinel. This trend is characterized by a large decrease of  $Cr/(Cr + Al)$  parallel to so-called olivine–spinel iso-potential lines. Similar trends of lesser magnitude and cyclic Al–Cr zoning have been identified in basaltic spinel. This trend is thought to be due to very rapid crystallization under conditions of supersaturation where the crystallization of spinel affects the local environment ahead of the growing spinel crystal (i.e. diffusion-controlled crystallization). The tendency for immiscibility between ferrite- or titanate-rich spinel, and aluminate-rich spinel (pleonaste) has a great influence on

Trends 1 and 3 zoning and also on atoll-spinel formation. Very local conditions such as nucleation, or lack of nucleation, of other minerals can influence both the textural environment and composition of kimberlitic spinel.

KEY WORDS: spinel; kimberlite; groundmass; zoning; zoning trends

## INTRODUCTION

Most diamonds have been transported to the Earth's surface by kimberlitic magma and thus the magmatic history may be important in understanding whether diamonds can survive the rapid journey from the upper mantle to the surface of the Earth. The term kimberlite is used in a very general sense that includes samples that might be better classified as ultramafic lamprophyres or lamproites (Rock, 1986; Mitchell, 1997; Tappe *et al.*, 2006). Composition and mineralogy has been used to divide kimberlites into Groups I and II (Dawson, 1967; Smith, 1983). Mitchell (1986, 1995) has described the differences in petrography and composition of these two groups and has used the terms kimberlite and orangeite to distinguish between Groups I and II respectively. We use the term kimberlite to cover both groups. Generally Group I kimberlites have a slightly lower content of potassium and much less phlogopite, and a higher content of groundmass oxide minerals (i.e. perovskite, ilmenite, spinel). Kimberlites generally contain evidence of significant late-stage volatile activity, particularly  $H_2O$  and  $CO_2$ , and this commonly leads to replacement of minerals that had crystallized earlier. There is evidence (Mitchell, 1986) that spinel commonly forms throughout kimberlite crystallization, thus the

\*Corresponding author. Telephone: (613) 533-6185. E-mail: roeder@geol.queensu.ca

morphology and composition of groundmass spinel may be useful in deciphering the kimberlite crystallization history. It has been shown by Pasteris (1980), Shee (1984), Hall (1991) and Naidoo *et al.* (2004) that the composition of the core of groundmass spinel can be useful in distinguishing different phases of kimberlite. We use the general term spinel to include all those oxide minerals with the spinel structure, such as chromite (Chr), magnesio-ulvöspinel-magnetite (Mum), magnesioferrite, pleonaste (Ple) and magnetite (Mag).

An understanding of the texture and chemical composition of kimberlite minerals is difficult because of the lack of detailed experimental work on the crystallization history of kimberlite magma and the possible role of liquid or fluid immiscibility (Mitchell, 1986, 1995). The kimberlite that we see is the end result of fairly rapid crystallization processes that start near 1200°C (Fedortchouk & Canil, 2004), with the early crystallization of olivine and spinel (Mitchell, 2006, 2008), and continue to temperatures well below 600°C (Armstrong *et al.*, 2004), at which point hydrous and carbonate minerals such as serpentine, pectolite, calcite and dolomite become stable phases.

A useful method to show the variation in composition of spinel is with the so-called spinel prism (Irvine, 1965; Haggerty, 1975; Mitchell & Clarke, 1976; Mitchell, 1986) using either ferric iron (oxidized prism) or titanium (reduced prism) as the vertical axis. However, it is difficult to visualize a large number of spinel analyses within this three-dimensional prism. Thus many researchers (e.g. Haggerty, 1975; Pasteris, 1980; Mitchell, 1986) have chosen to plot the spinel analyses as if projected onto the three bounding planes of the spinel prism. Figure 1 is a plot of almost 3000 published spinel analyses from kimberlites and related rocks as if projected onto the right-hand face of the oxidized spinel prism. These published spinel analyses and references are given in Electronic Appendix 1 (available for downloading at <http://www.petrology.oxfordjournals.org>). Mitchell (1986) used this projection to identify two distinct compositional trends as shown by Trends 1 and 2 in Fig. 1. Mitchell (1986) pointed out that Trend-1 spinel is commonly from Group-I kimberlites and Trend-2 spinel tends to be associated with Group-II kimberlites (orangeites), although Mitchell (1986) identified a number of exceptions.

Spinel macrocrysts and xenocrysts in kimberlites (dark grey circles in Fig. 1) are derived from the breakup of upper-mantle peridotite, and are then transported to the surface by kimberlitic magma. These spinel macrocrysts and xenocrysts that are low in  $\text{Fe}^{2+}/(\text{Fe}^{2+} + \text{Mg})$  tend to be low in both titanium ( $\text{TiO}_2 < 1$  wt %) and ferric iron. There are some macrocrysts with higher  $\text{Fe}^{2+}/(\text{Fe}^{2+} + \text{Mg})$  that are Cr-, Ti- and  $\text{Fe}^{3+}$ -rich that are thought to be derived from metasomatized upper-mantle peridotite (Schulze, 2001).

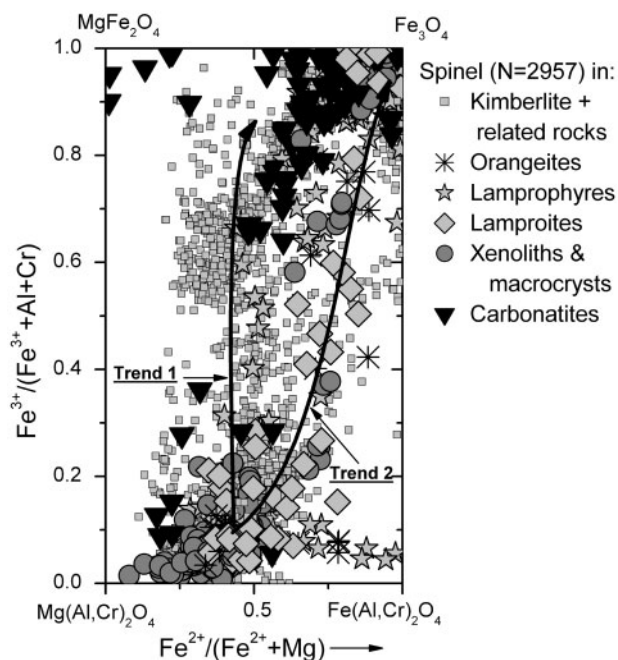


**Fig. 1.**  $\text{Fe}^{3+}/(\text{Fe}^{3+} + \text{Al} + \text{Cr})$  vs  $\text{Fe}^{2+}/(\text{Fe}^{2+} + \text{Mg})$  for published spinel from kimberlites and related samples. See Electronic Appendix 1 for spinel analyses and references. Curves of Trend 1 and 2 are after Mitchell (1986).

The trends of spinel composition in kimberlites have been explained using a number of mechanisms. Mitchell (1986) explained Trend 2 as due to the early crystallization of phlogopite, which reduces both Al and Mg in the melt, thus increasing both the  $\text{Fe}^{3+}/(\text{Fe}^{3+} + \text{Al} + \text{Cr})$  and  $\text{Fe}^{2+}/(\text{Fe}^{2+} + \text{Mg})$  in spinel. Mitchell (1986) explained the different  $\text{Fe}^{2+}/(\text{Fe}^{2+} + \text{Mg})$  of spinel at the beginning of the trends as due to spinel derived from slightly different parent compositions that may be produced by magma mixing, whereas Pasteris (1980) explained these varying trends by different degrees of differentiation. Wall-rock contamination of kimberlite magma may also play a role as shown by pleonaste spinel (Pasteris, 1980; Chakhmouradian & Mitchell, 2001).

Analyses of spinel in kimberlites are commonly compared with analyses of spinel in volcanic rocks, principally basalt. The trend of basaltic spinel in a  $\text{Fe}^{3+}/(\text{Fe}^{3+} + \text{Al} + \text{Cr})$  vs  $\text{Fe}^{2+}/(\text{Fe}^{2+} + \text{Mg})$  diagram is similar to Trend 2 for kimberlitic spinel (Mitchell, 1986; Barnes & Roeder, 2001). The basaltic trend is mainly due to the crystallization during cooling of olivine, plagioclase and clinopyroxene that increases  $\text{Fe}^{3+}/(\text{Fe}^{3+} + \text{Al} + \text{Cr})$  in the residual magma as a function of increasing  $\text{Fe}^{2+}/(\text{Fe}^{2+} + \text{Mg})$ . A common feature of both kimberlitic and basaltic spinel is that early spinel is very chromian rich (chromite or chromian spinel) and later spinel is very chromian poor. Thus the early spinel is near the base and the later spinel is near the top of the oxidized and reduced

spinel prisms. Whereas there is no sign of Trend 1 in basaltic spinel, this trend is the dominant trend of kimberlites (Fig. 1).

Roeder *et al.* (2006) examined the variation in spinel composition in a number of basalts that had been quenched rapidly enough to preserve the composition of the melt as glass. Some of these spinel crystals are strongly zoned, particularly with respect to Cr and Al. Roeder *et al.* (2001, 2003, 2006) concluded that a change in conditions to supersaturate the melt in spinel may have caused diffusion-controlled crystallization and thus significant Cr–Al zoning in the crystals. The zoning in the crystals therefore may be due to a very local effect caused by depletion of chromium in the immediate vicinity of the rapidly growing crystals and may not necessarily represent a major change in the bulk chemistry of the melt.

The major focus of the present study was to analyze the composition of groundmass spinel from a number of kimberlites in order to relate the composition of the spinel to the morphology and petrographic environment of the spinel. An important part of this study was to identify spinel zoning trends in the kimberlite groundmass and to relate these trends to crystallization processes of the kimberlite.

## ANALYTICAL TECHNIQUES

The electron-microprobe analyses of spinel (Electronic Appendix 1) were made by energy-dispersive spectrometry using a technique described by Roeder *et al.* (2001, 2006). Quality control was maintained by analyzing a standard chromite (USNM 117075) during each electron-microprobe session. The resulting average wt% oxide for USNM 117075, the standard deviation of 151 analyses and the listed (Jarosewich *et al.* 1980) values for each oxide are as follows:  $\text{Al}_2\text{O}_3$  (10.26, 0.32, 9.92),  $\text{Cr}_2\text{O}_3$  (60.21, 0.32, 60.5),  $\text{FeO}$  (12.97, 0.25, 13.04),  $\text{MnO}$  (0.19, 0.20, 0.11),  $\text{MgO}$  (15.31, 0.31, 15.20). The proportion of  $\text{Fe}^{2+}$  and  $\text{Fe}^{3+}$  in spinel was calculated assuming spinel stoichiometry. Most of the spinel grains are small ( $<100\text{ }\mu\text{m}$ ) and often show considerable compositional variation over  $5\text{--}20\text{ }\mu\text{m}$ . Thus the spatial resolution of the electron microprobe analysis is important in order to determine the discontinuity in composition between adjoining zones. All spinel analyses were made with an electron-beam diameter smaller than  $1\text{ }\mu\text{m}$ ; however, the effective diameter of the analysed volume is much larger ( $\sim 3\text{--}20\text{ }\mu\text{m}$ ). The diameter of the analyzed volume depends on the element analyzed, the other elements present in an adjoining zone and the secondary fluorescence of X-rays in a nearby zone. Secondary fluorescence is a particular problem between zones with major differences in Fe, Cr and Ti, which is often the case in adjoining zones in kimberlite spinel. Many crystals show by X-ray mapping an abrupt ( $<2\text{ }\mu\text{m}$ ) discontinuity between zones that reflects an abrupt chemical

discontinuity. However, electron microprobe analysis may show a virtual chemical variation within  $5\text{--}20\text{ }\mu\text{m}$  of the discontinuity because of secondary fluorescence. This secondary fluorescence involves Fe X-rays produced under the electron beam in one zone exciting Cr and Ti X-rays in an adjoining zone.

## SAMPLES AND PETROGRAPHY

The samples used in the present study are listed in Table 1 and have come from 46 kimberlite localities, mainly from the hypabyssal and volcanoclastic facies. The present study is not meant to duplicate studies that have analyzed spinel in multiple samples of single kimberlites, such as those studies that led to the data shown in Fig. 1. Rather, the present work is a detailed comparative study of a small number of samples from single kimberlites. The detailed petrography of these kimberlites has been described in various publications, some of which are listed in Table 1. No attempt is made to undertake detailed petrography of single samples but we discuss those characteristics that are important to an understanding of spinel crystallization. The petrographic atlas published by Mitchell (1997) is highly recommended for an overview of the petrography of kimberlites.

Almost all the samples contain rounded olivine macrocrysts, the majority of which are serpentinized. A few samples (e.g. Tunraq and Kirkland Lake) contain very fresh olivine macrocrysts and small unaltered euhedral microphenocrysts of olivine in which only the rims are partially serpentinized. Some olivine macrocrysts contain euhedral spinel inclusions (Fig. 2a). In many cases, these samples contain in the groundmass translucent red anhedral spinel fragments surrounded by an opaque rim of chromite (Fig. 2b) and magnesio-ulvöspinel–magnetite. The translucent spinel crystals are low in  $\text{TiO}_2$  ( $<1\text{ wt } \%$ ) consistent with macrocrysts (Fig. 1) and are assumed to be disaggregated spinel peridotite that formed prior to inclusion in kimberlitic magma. Other less common macrocryst phases are garnet, ilmenite and phlogopite. Samples with ilmenite macrocrysts commonly contain ilmenite fragments in the groundmass that are surrounded by irregular rims of perovskite and titaniferous magnetite. The most common minerals of the groundmass that crystallized from the kimberlite magma, or derived solutions, are olivine, phlogopite, spinel, ilmenite, perovskite, monticellite, apatite, calcite, dolomite, pectolite and serpentine. Some kimberlites contain laths of phlogopite or calcite that are aligned (Fig. 2c) indicating flowage of the groundmass. Phlogopite is usually a major mineral in Group II kimberlites whereas spinel is a very minor phase. Some phlogopite laths have a fairly clear core with an outside rim containing small spinel and perovskite crystals. Some phenocrysts of olivine contain perovskite and spinel arranged in zones (Fig. 2d). As noted by Mitchell (1986), atoll spinel (Fig. 2e) is found in some Group I kimberlite

Table 1: *Kimberlite and related rock samples*

Sample	Location	Description	Sample donor	Reference
23rd Party Congress	Siberia, Russia	Tuffisitic	J. J. Brummer	Lapin <i>et al.</i> (2007)
Benfontein	Kimberley, SA	Dike (sill), phase layered	B. Dawson	Dawson & Hawthorne (1973)
Blaauwbosch (II)	Boshof, SA	Hypabyssal	D. Schulze	Ford (1987)
Blue Hills	Namibia	Hypabyssal	S. Kurszlaukis	Kurszlaukis & Franz (1998)
Bobbejaan (II)	Bellsbank, SA	Hypabyssal	D. Schulze	Boctor & Boyd (1982)
Bufonta	Kirkland Lake, ON, CA	Hypabyssal	K. Barron	Barron & Barnett (1993)
Certac	Val d'Or, QUE, CA	Hypabyssal dike in gold mine	D. Schulze	Van Rythoven (2006)
Chicken Park	Colorado, USA	Hypabyssal	B.C. Hearn	Coopersmith <i>et al.</i> (2003)
Colossus	Zimbabwe	Hypabyssal	Miller Museum	Allsopp <i>et al.</i> (1985)
Dixonville	Tonoma, PA, USA	Hypabyssal	D. Schulze	Doden <i>et al.</i> (1998)
Eendrag (II)	Barkly West, SA	Hypabyssal	D. Schulze	Schulze (2001)
Ekati (Grizzly Pipe)	Slave, NWT, CA	Hypabyssal	8th IKC sample	Nowicki <i>et al.</i> (2004)
Frank Smith	Barkly West, SA	Hypabyssal	D. Schulze	Bell & Mofokeng (1998)
Forte a La Corne, pipe 150	Saskatchewan, CA	Volcanoclastic	C. Hetman	Scott Smith <i>et al.</i> (1995)
Igwis Hills	Tanzania, Africa	Volcanoclastic and lava	B. Dawson	Reid <i>et al.</i> (1975)
Iron Mt.	Wyoming, USA	Hypabyssal	D. Schulze	Smith <i>et al.</i> (1979)
Ison Creek	Kentucky, USA	Hypabyssal	D. Schulze	Agee <i>et al.</i> (1982)
Ithaca deposits	Ithaca, NY, USA	Dikes and varied	D. Schulze	Martens (1924)
Jagersfontein	Jagersfontein, SA	Hypabyssal	D. Schulze	Taylor & Kingdom (1999)
Jericho	Slave, NWT, CA	Hypabyssal	M. Kopylova	Price <i>et al.</i> (2000)
Jos Dike	Somerset, Island, CA	Hypabyssal	B. Kjarsgaard	Mitchell & Meyer (1980)
Kikerk	Nunavut, CA	Hypabyssal	M. Manson	None
Kirkland Lake	Ontario, CA	Hypabyssal	J.J. Brummer	Armstrong <i>et al.</i> (1997)
Lace (II)	Free State, SA	Hypabyssal	D. Schulze	Schulze (2001)
Leicester Mine	Barkly West, SA	Hypabyssal	D. Schulze	Schulze (2001)
Los Indios Sill	Guaniamo, Venezuela	Sill	D. Channer	Kaminsky <i>et al.</i> (2004)
Majuagaa	West Greenland	Dike	D. Kamenetsky	Nielsen <i>et al.</i> (2006)
Masontown	Pennsylvania, USA	Dike	D. Schulze	Hunter <i>et al.</i> (1984)
Monastery Mine	Free State, SA	Hypabyssal	D. Schulze	Whitelock (1973)
New Elands (II)	Boshof, SA	Hypabyssal	D. Schulze	Mitchell & Meyer (1989)
Newlands (II)	Barkly West, SA	Hypabyssal	D. Schulze	Becker & le Roex (2006)
Nix	Colorado, USA	Hypabyssal	D. Schulze	Coopersmith <i>et al.</i> (2003)
Paul Lake	Lac de Gras, Slave, NWT, CA	Hypabyssal	B. Kjarsgaard	Kjarsgaard & Wyllie (1993)
Picton Quarry	Ontario, CA	Dike	L. Godin	Arima & Kerrien (1988)
Rex Mine (II)	Free State, SA	Hypabyssal	D. Schulze	Hill (1989)
Rich	Slave, NWT, CA	Hypabyssal	B. Paniatowsky and J. Crawford	Crawford (2003)
Roberts Victor (II)	Boshof, SA	Hypabyssal	D. Schulze	MacGregor & Carter (1970)
Sarfartoq	West Greenland	Hypabyssal	C.H. Hetman	Jensen & Secher (2003)
Sloan	Colorado, USA	Hypabyssal	D. Schulze	McCallum & Egglar (1971)
Snap Lake	Slave, CA	Dike	8th IKC sample	Mogg <i>et al.</i> (2003)
Star (II)	Free State, SA	Hypabyssal	D. Schulze	Mitchell & Meyer (1989)
Tli Kwi Cho	Slave, NWT, CA	Pyroclastic facies	C. Jennings	Doyle <i>et al.</i> (1999)
Tunraq	Somerset Is., NWT, CA	Breccia	B. Kjarsgaard	Mitchell (1979)
Udachnaya	Yakutia, Russia	Hypabyssal	D. Kamenetsky	Kamenetsky <i>et al.</i> (2008)
Wemindji	Quebec, CA	Hypabyssal	D. Schulze	Mitchell & Letendre (2003)
Wesselton	Kimberley, SA	Hypabyssal	D. Schulze	Shee (1984)

CA, Canada; SA, South Africa; IKC, International Kimberlite Conference.

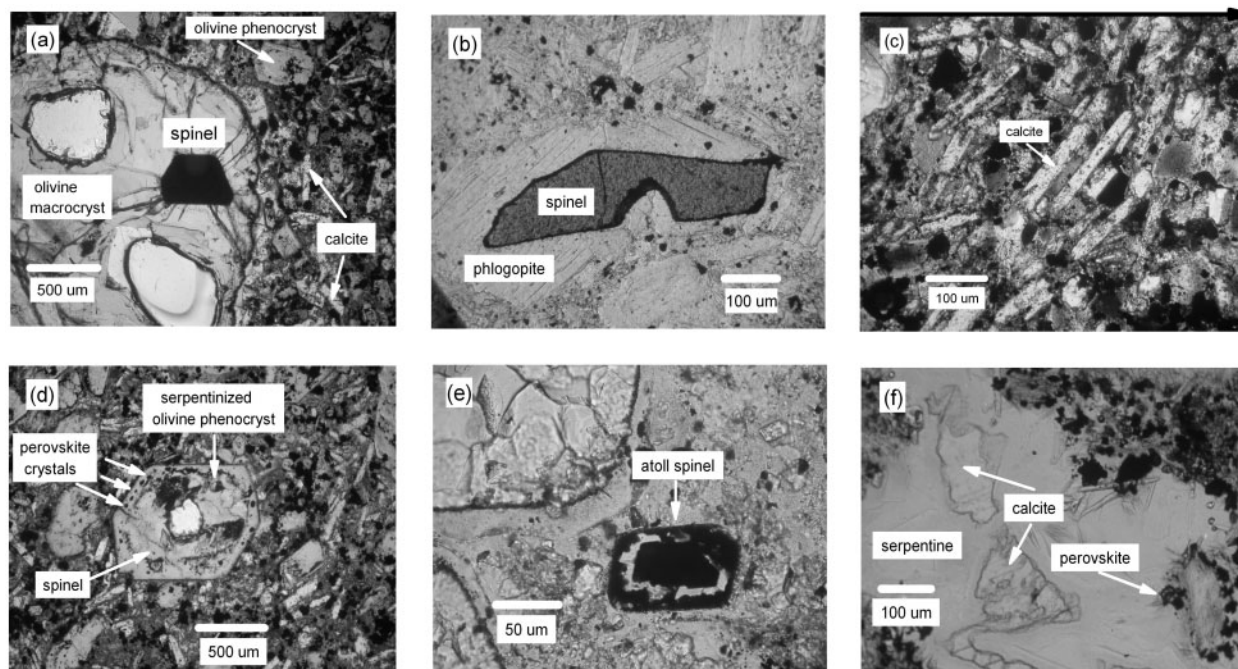


**Fig. 2.** Transmitted-light photomicrographs. (a) Serpentinized olivine macrocryst enclosing a euhedral spinel grain surrounded by radiating contraction cracks. Tunraq K10B. (b) Spinel macrocryst with narrow opaque rim of chromite partially enclosed by groundmass phlogopite. Opaque rim is thickest in reentrant where spinel is not covered by phlogopite. Casadilla Gorge, Ithaca. (c) Oriented laths of calcite. 23rd Party Congress, Russia. (d) Serpentinized olivine phenocryst with a spinel inclusion and a rim containing enclosed perovskite crystals. Tunraq, K10B. (e) Atoll spinel with calcite and serpentine in the lagoon between the core and the rim. 23rd Party Congress. (f) Segregation of serpentine and calcite. Wesselton, W-2.

but is rare in Group II kimberlite. The atoll 'lagoons' are usually composed of serpentine and/or calcite.

One of the most puzzling aspects of kimberlite petrology is the role that serpentine and carbonate play in the crystallization of the groundmass. Some kimberlites have a groundmass that is largely serpentine and carbonate and it is not known whether these are alteration products, and thus represent replacement of earlier minerals, or whether the serpentine and carbonate crystallized directly from a melt, gel or fluid phase. Many Group I kimberlites contain calcite or carbonate segregation textures (Mitchell, 1997; Armstrong *et al.*, 2004). These are irregular amoeboid bodies (Fig. 2f) composed largely of serpentine, in some cases with carbonate cores, and a rim with large carbonate crystals, prismatic apatite and phlogopite crystals projecting inward from the segregation rim. We have also found in the segregations amoeboid hydrous Ca, Fe and Ti silicates that may represent either a new mineral or a variant of atwillite. This unknown mineral is also found in the 'lagoon' of some atoll spinel.

## SPINEL ANALYSES

The spinel analyses of the present study are given and described in Electronic Appendix 1, and are plotted in

Figs 3–5. The spinel analyses from Group II kimberlites are shown with blue symbols whereas the other colour symbols represent spinel from either Group I or unclassified kimberlites and related rocks. Discussion of the wide range in composition of kimberlite spinel is made easier by identifying six common groups of spinel or stages of growth of spinel. These are xenocryst peridotite spinel (Xen), metasomatized xenocryst peridotite spinel (Xen'), chromite (Chr), pleonaste spinel (Ple), magnesio-ulvöspinel–magnetite (Mum) and magnetite (Mag). The boundaries for these groups are of necessity arbitrary and these groups are intended only for ease of discussion. These fields are consistent with the spinel types identified by previous workers (i.e. Mitchell, 1986, 1995; Haggerty, 1975; Edwards *et al.*, 1992). Figure 3 shows a projection onto the base of both the so-called oxidized- and reduced-spinel prism. Included in Fig. 3 are two lines that represent so-called iso-potential lines (Irvine, 1965) of spinel in equilibrium with olivine at a constant temperature. The iso-potential lines represent the composition of spinel that is in equilibrium with olivine (FO 90 and 80) at a constant temperature of 1200°C and 1100°C. The variable  $\text{Fe}^{3+}$  and Ti in spinel has not been taken into consideration in calculating these lines, thus these lines cannot be used in a quantitative sense. The lines were calculated using the equations

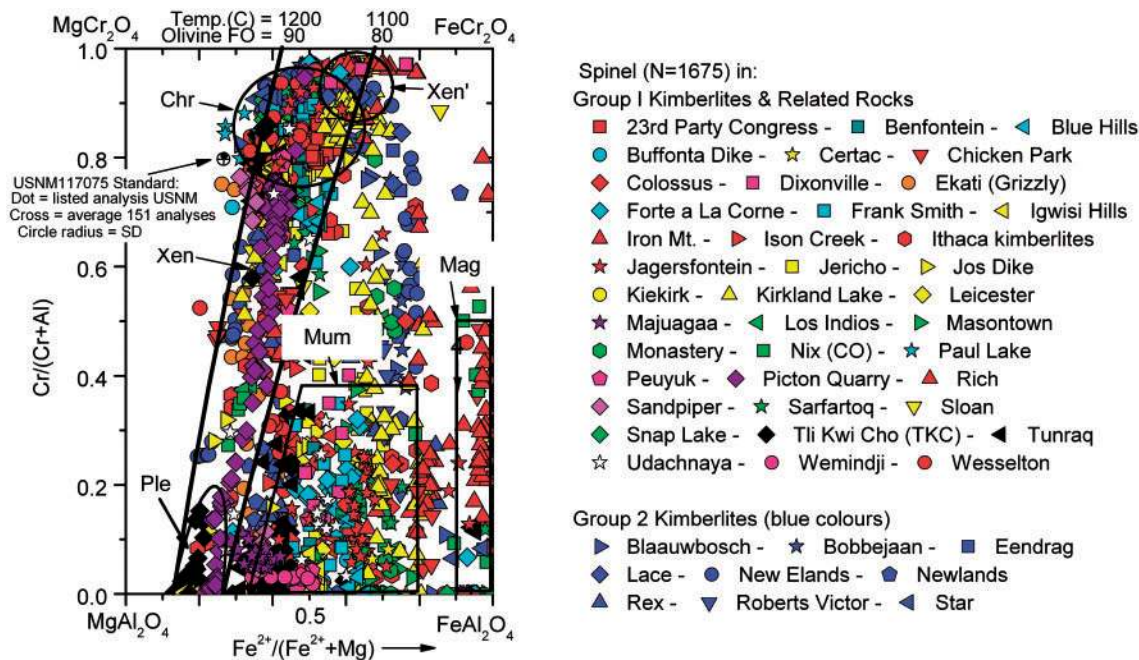


**Fig. 3.**  $\text{Cr}/(\text{Cr}+\text{Al})$  vs  $\text{Fe}^{2+}/(\text{Fe}^{2+}+\text{Mg})$  for spinel in kimberlites of the present study. Blue symbols for spinel in Group II kimberlites. The fields Xen, Xen', Chr, Mum, Ple and Mag are outlined to facilitate discussion in the text. Spinel analyses and information on single kimberlites are given in Electronic Appendix 1. The USNM 117075 chromite standard was analyzed during each electron-microprobe session.

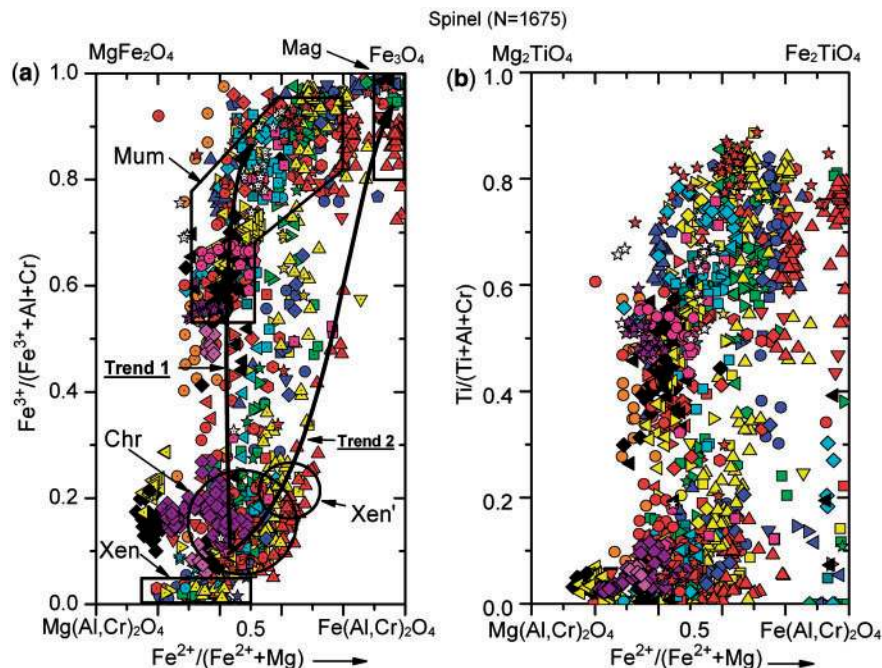


**Fig. 4.** (a)  $\text{Fe}^{3+}/(\text{Fe}^{3+}+\text{Al}+\text{Cr})$  and (b)  $\text{Ti}/(\text{Ti}+\text{Al}+\text{Cr})$  vs  $\text{Fe}^{2+}/(\text{Fe}^{2+}+\text{Mg})$  for spinel in kimberlites of the present study. Legend for symbols given in Fig. 3.

of Pousovetov (2000). It should be noted that very few spinel analyses plot to the left of the 1200°C and FO = 90 line and most of the Xen, Chr and Ple spinel analyses lie between the two lines. Figure 4 shows the variation

of ferric iron and titanium in the spinel. The relative distribution of analyses of the present study in Fig. 4a is similar to the distribution of published analyses shown in Fig. 1. The boundaries of the labeled fields in Fig. 4a are drawn

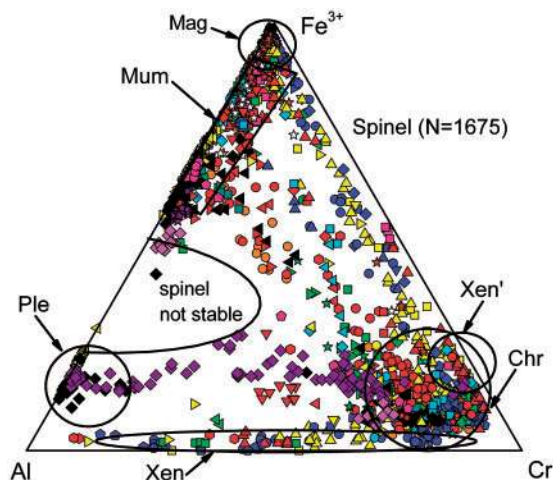


**Fig. 5.** Al–Cr–Fe<sup>3+</sup> for spinel in kimberlites of the present study. Legend for symbols given in Fig. 3.

arbitrarily and are not consistent between different projections and thus are not shown on Fig. 4b. The identified fields can be thought of as different stages of spinel crystallization. Some spinel crystals show a sharp compositional discontinuity between three stages. The Xen field includes translucent red spinel macrocrysts derived from peridotites that are either totally enclosed in large olivine macrocrysts or form the core of spinel fragments that were transported by the kimberlitic magma to the surface. The Xen field overlaps in some projections a field of fairly late-stage aluminous spinel (Ple) that is described in a later section.

The Chr field includes the largest concentration of spinel high in chromium and this spinel often forms the small euhedral core of groundmass spinel or is included in olivine phenocrysts. These spinel are thought (Mitchell, 2006, 2008) to be the first spinel (primary) to have crystallized directly from the kimberlitic magma, either in the upper mantle or during the passage of the kimberlitic magma to the surface of the Earth. The majority of the spinel analyses in the Chr field (Figs 3, 4a and 5) are surrounded by Mum spinel that Mitchell (1986) has described as being on Trend 1 (magnesio-ulvöspinel–magnetite trend). There is, however, a significant number of spinel analyses that fall between the Chr and Mum fields. These analyses may reflect an actual transition between the two zones of the crystal or reflect microprobe analyses that overlap two distinct zones of the crystal because of the discrete analyzing volume sampled by the electron microprobe. Careful examination of some of the spinel crystals by X-ray mapping has shown that some of the spinel analyses that fall between the Chr and Mum fields may in fact overlap two distinct zones in the crystal because of secondary fluorescence. The Mag stage includes almost pure magnetite, some of which may have formed well below the solidus temperature of the kimberlite magma and may be the result of late fluids that were involved in

serpentinization of olivine and the formation of carbonate segregations.

Comparison of Fig. 4a and b suggests that ferric iron and titanium tend to show similar trends except for the late magnetite (Mag in Fig. 4a), which is usually very low in titanium. The primary Chr spinel not only has low Fe<sup>3+</sup>/(Fe<sup>3+</sup> + Al + Cr) but also low Ti/(Ti + Al + Cr), whereas the Mum spinel with high Fe<sup>3+</sup>/(Fe<sup>3+</sup> + Al + Cr) usually has high Ti/(Ti + Al + Cr) above 0.4.

The ternary projection of the so-called oxidized spinel prism is shown in Fig. 5. There are many fewer spinel analyses on the left-hand side between the aluminous- and ferrite-rich spinel. This is due to the incompatibility of Al with Fe<sup>3+</sup> in the spinel structure at the temperatures at which these spinel grains formed. The boundary of the area marked 'spinel not stable' in Fig. 5a is variable and depends on both temperature (Sack & Ghiorso, 1991) and the variation of Fe<sup>2+</sup>, Mg and Ti in the spinel. One has to keep in mind that these two-dimensional diagrams are in fact projections and thus points plotting at the same position in Fig. 5 may have very different Fe<sup>2+</sup>/(Fe<sup>2+</sup> + Mg) and Ti and thus a different field of stability at a particular temperature. It is also noted that in the very dynamic conditions prevalent during kimberlite evolution the range of spinel composition may extend outside that expected for equilibrium conditions and thus some spinel grains may have formed metastably.

## SPINEL TRENDS WITHIN SINGLE KIMBERLITES

It is not feasible to show the chemical trend and textural environment of spinel in all the studied kimberlites so only a few examples (Figs. 6–14) are presented, to illustrate particular points that are common to spinel trends in more than one kimberlite. We have also arbitrarily chosen to concentrate on the variation of Fe<sup>3+</sup>, and not on Ti; however, a plot of Ti/(Ti + Al + Cr) vs Fe<sup>2+</sup>/(Fe<sup>2+</sup> + Mg) of the reduced spinel prism for Figs 6–14 is available in Electronic Appendix 1.

The spinel trends for three Group I kimberlites that show a wide range of spinel composition are compared in Fig. 6a and b. The Grizzly (Ekati) spinel grains follow Trend 1 and are the most magnesian spinel found in the present study. In contrast, the Rich spinel grains have the highest Fe<sup>2+</sup>/(Fe<sup>2+</sup> + Mg) and are seemingly the best example of Trend 2 found in the present study. The Jericho spinel data fall between Trends 1 and 2. The very small, but important, difference in Fe<sup>2+</sup>/(Fe<sup>2+</sup> + Mg) values (*c.* 0.4, 0.5, 0.6) at low values of Fe<sup>3+</sup>/(Fe<sup>3+</sup> + Al + Cr) of the Chr spinel in the three kimberlites are noted. Minor differences of Fe<sup>2+</sup>/(Fe<sup>2+</sup> + Mg) in Chr spinel for the three kimberlites seem to become magnified as the spinel changes from Chr to Mum composition. The Grizzly spinel grains are not

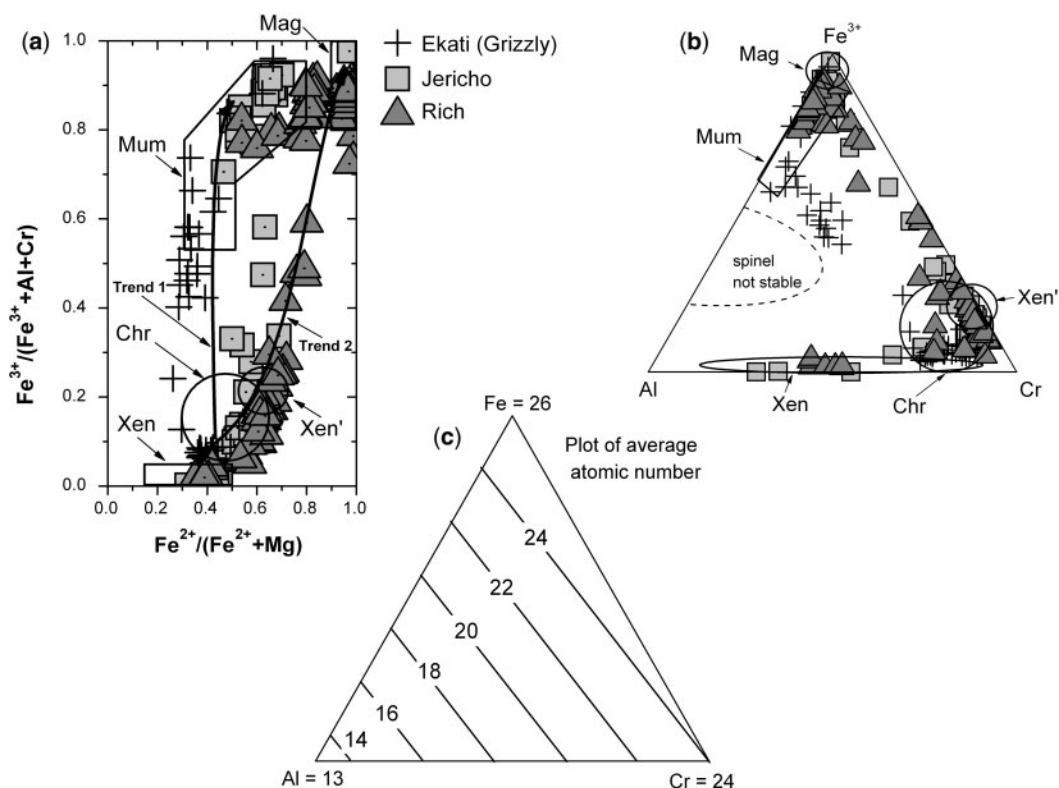


**Fig. 6.** (a)  $\text{Fe}^{3+}/(\text{Fe}^{3+} + \text{Al} + \text{Cr})$  vs  $\text{Fe}^{2+}/(\text{Fe}^{2+} + \text{Mg})$  for Grizzly (Ekati), Jericho and Rich spinel. (b) Al–Cr– $\text{Fe}^{3+}$  for Grizzly (Ekati), Jericho and Rich spinel. (c) Ternary diagram showing lines of constant average atomic number for Al, Cr and Fe.

only the most magnesian (Fig. 6a) but also the most aluminous (Fig. 6b). Both the Jericho and Rich kimberlite contain spinel xenocrysts (field Xen), a few of which have a core that may be a metasomatized upper-mantle peridotite (Xen') surrounded by primary chromite (Chr).

The primary method used by most workers to distinguish different zones of spinel is by using the contrast in back-scattered electron (BSE) imaging, which essentially depends upon differences in average atomic number (AN) of the zones. Because of spinel-crystal chemistry the low atomic number elements Mg (AN = 12) and Al (AN = 13) tend to co-vary, as do the higher atomic number elements Cr (AN = 24) and Fe (AN = 26). Thus zones of different Al and Cr show a large BSE contrast whereas zones of significantly different Cr and Fe show little or no BSE contrast. Lines of constant average atomic number for the Al–Cr–Fe ternary diagram are shown in Fig. 6c. These lines can also be thought of as lines of constant BSE imaging.

As the location chosen for an electron-microprobe analysis is usually guided by differences seen in BSE images, it is often impossible to differentiate by BSE imaging the Chr and Mum zones for both Trends 1 and 2 spinel because these trends are almost parallel to lines of constant average atomic number (compare Fig. 6b and 6c). Thus some microprobe analyses that lie between the Chr and Mum

fields may transgress two zones that were not recognized at the time of analysis. This applies to both the present study and published studies.

The large range of zoning found in single spinel crystals from Rich is shown in Fig. 7 by lower-case letters and tie lines. Lower-case letters are used in succeeding diagrams to indicate a position on a single spinel crystal. Point a on the three projections is shown within a rectangular box to facilitate comparison between the three projections. A noteworthy feature is the large contrast in back-scattering response between points a and b in Fig. 7d and the small BSE contrast between points b and c considering the large difference in composition. The core of the spinel (point a) in Fig. 7d is a spinel xenocryst that is surrounded by chromite (b) and magnesio-ulvöspinel–magnetite (c) over a distance of 25  $\mu\text{m}$ . One distinctive feature of spinel in different samples of the Rich kimberlite is a very narrow outer zone (i.e. point f in Fig. 7e) that has a significantly lower  $\text{Fe}^{2+}/(\text{Fe}^{2+} + \text{Mg})$  at  $\text{Fe}^{3+}/(\text{Fe}^{3+} + \text{Al} + \text{Cr}) = 0.8$  (Fig. 7b). We ascribe this very narrow outer zone to a high Mg activity at a very late stage as indicated by the large amount of late-stage dolomite in the groundmass. Tie lines with arrows are shown in Fig. 7b for four crystals that display zoning to an outer magnesian rim (i.e. point f). The Rich spinel seems to follow Trend 2 except for this

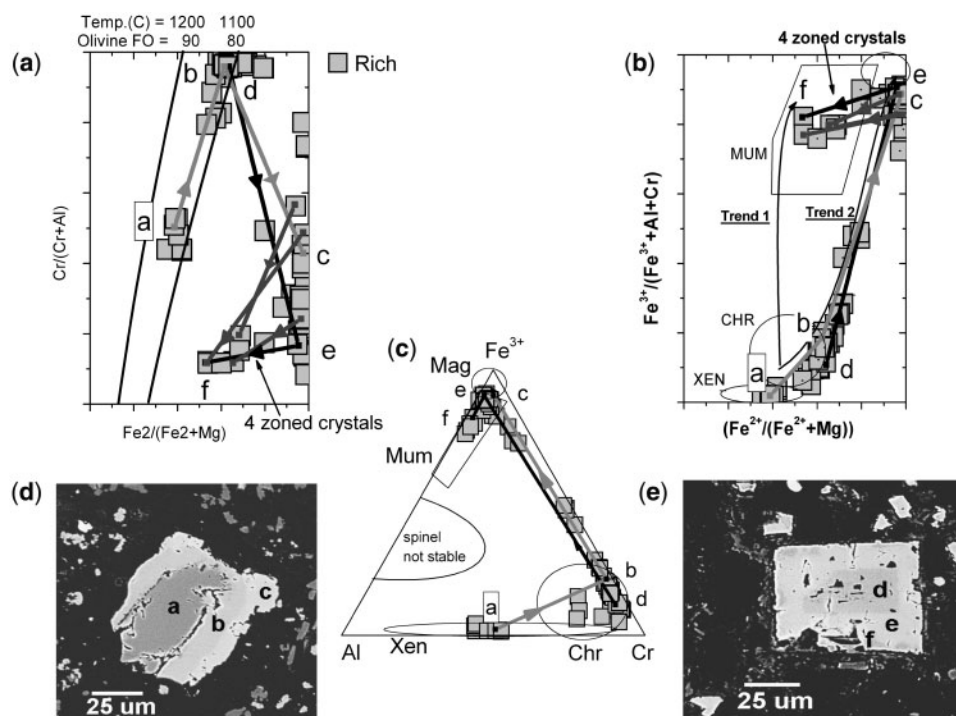


**Fig. 7.** (a–c) Three projections of oxidized spinel prism for Rich spinel. Lines with arrows show zoning trends. Lower-case letters indicate analyses for points on the BSE images. (d, e) BSE images.

late-stage outer rim that extends toward Trend 1 (Fig. 7b). The spinel in Fig. 7e has a core (d) that is consistent with primary spinel that crystallized from the kimberlitic magma and shows extreme zoning to the outermost magnesian rim (f). A subtle outermost magnesian rim also occurs in some Jagersfontein and Grizzly spinel. Masun (1999) described a more magnesian rim on occasional magnetite from some Lac de Gras kimberlites.

An example of why one has to be very careful in ascribing an origin for spinel that plots in a certain position within one of the projections is the position of point a in Fig. 7a–c. This spinel is obviously a spinel xenocryst in field Xen in all three projections and thus this spinel was derived from a peridotite that predated inclusion in the kimberlitic magma. Compare this to the zoning of Grizzly spinel shown in Fig. 8. Note the position of point b (surrounded by a rectangular box) in Fig. 8a–c. Although point b in Fig. 8a lies in the same position in the Xen field as point a in Fig. 7a, the  $\text{Fe}^{3+}$  is very high for point b and this spinel lies between fields Chr and Mum in Fig. 8b and c and thus is not a xenocryst. The spinel in Fig. 8d shows very small holes between b and c that may represent an incipient ‘lagoon’ in an atoll. Note the relatively large contrast in electron back-scattering between points m, n and o in Fig. 8e, considering the small difference in the  $\text{Cr}/(\text{Cr} + \text{Al})$  between these three points. The repetition of the m, n and o zones that parallel the iso-potential curves

in Fig. 8a are a common feature in spinel from several kimberlites. This type of zoning is also common in mid-ocean ridge basalt (MORB) spinel (Roeder *et al.*, 2001), but at lower values of  $\text{Cr}/(\text{Cr} + \text{Al})$ .

Spinel analyses from the New Elands kimberlite (Group II) are shown in Fig. 9. The trend for most of the spinel analyses (black circles) is compatible with Trend 2 (Fig. 9b) except for the circled analyses (light-grey circles) of a unique crystal shown in Fig. 9d and e. Analyses of this crystal have been grouped into four distinct zones (circled), labeled a, b, c, and d. The core (zone a) of this crystal is typical of a xenocryst derived from peridotite with 0.7 wt %  $\text{TiO}_2$  and high in  $\text{Al}_2\text{O}_3$  and  $\text{Cr}_2\text{O}_3$ . The zoning from a to c is to lower Cr (Fig. 9c) with  $\text{Al}_2\text{O}_3$  increasing from 11 wt % in the core (a) to 44 wt %  $\text{Al}_2\text{O}_3$  in c. It should be noted that this zoning from a to c is parallel (arrows) to the 1200°C iso-potential line in Fig. 9a. The extreme outer zone d is low in  $\text{Al}_2\text{O}_3$  like most late-stage spinel. No other crystals were found in seven New Elands thin sections that showed a similar compositional variation or atoll morphology. Indeed, as noted by Mitchell (1986), it is rare to find atoll spinel in any Group II kimberlites. The aluminous spinel (zone c) is found only in the lower part of the crystal, where there is a lagoon filled with serpentine. This aluminous spinel seems to occur only at the corners of the crystal. There is a sharp discontinuity between the d zone and the rest of the

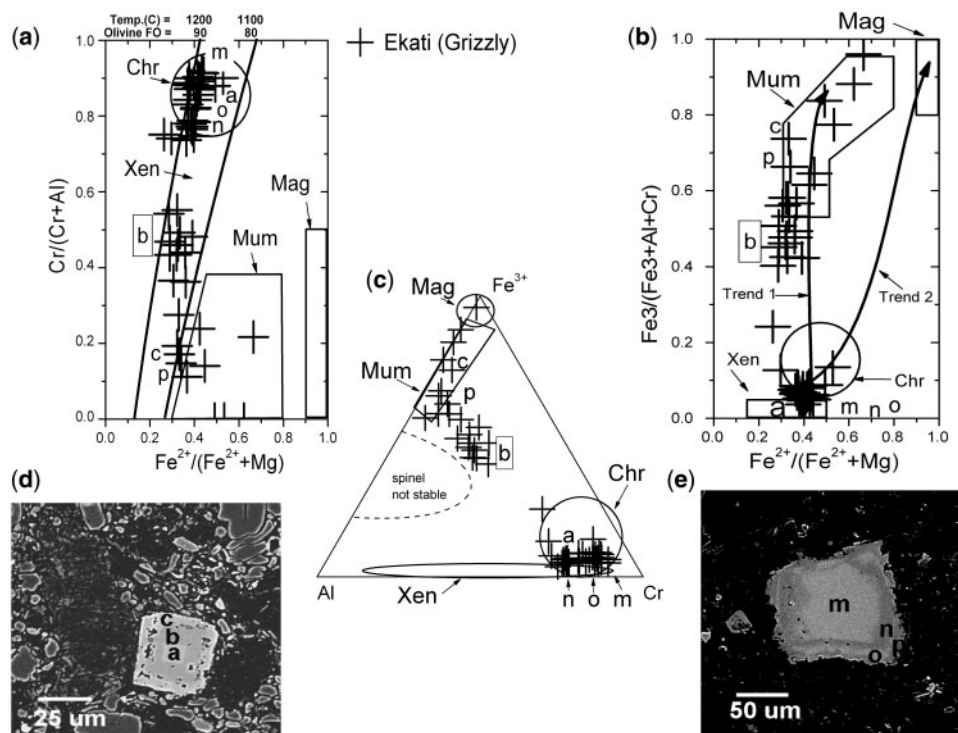


**Fig. 8.** (a–c) Three projections of oxidized spinel prism for Ekati (Grizzly) spinel. (d, e) BSE images.

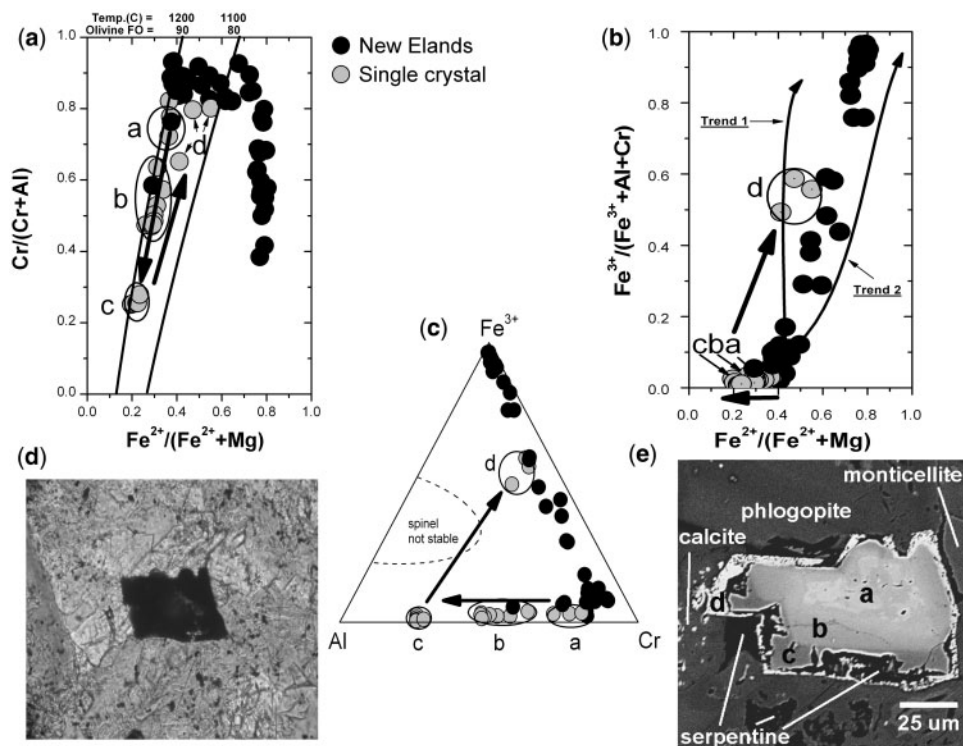


**Fig. 9.** (a–c) Three projections of oxidized spinel prism for New Elands spinel. (d) Transmitted light image of unique spinel. (e) BSE image of unique spinel in (d). There are four identifiable zones (a, b, c, d) on this unique crystal and the circles in parts (a–c) of this figure enclose a number of analyses (light grey circles) for each zone. Arrows indicate direction of zoning for the unique crystal.

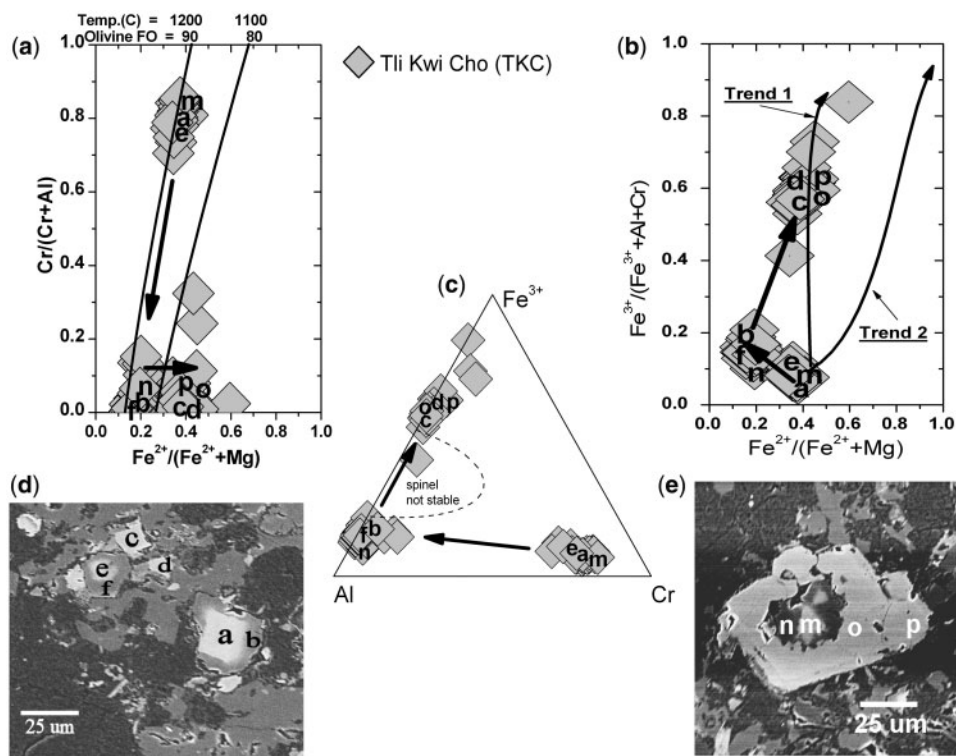


**Fig. 10.** (a–c) Three projections of oxidized spinel prism for Tli Kwi Cho spinel. Arrows indicate direction of zoning. (d, e) BSE images.

spinel, as seen in the BSE image, and a distinct compositional break between the c and d zones.

The spinel from the Tli Kwi Cho (TKC) pyroclastic kimberlite is shown in Fig. 10. A number of spinel grains in this sample show a remarkable range in  $\text{Cr}/(\text{Cr}+\text{Al})$  from 0.8 (a, m) to less than 0.1 (b, n) over a distance of less than 5  $\mu\text{m}$ . The zoning of TKC crystals is indicated by the arrow that is parallel to the 1200°C iso-potential line in Fig. 10a. The difference in electron back-scattering between the core (a and e) and rim (b and f) in Fig. 10d is very large but diffuse. This suggests that the boundary is continuous (i.e. a–b and e–f) in composition but too small to measure because of the overlapping analytical volumes. Crystals having a composition of c and d are present as separate crystals. The sharp boundary (Fig. 10e) between n and o should be noted, which separates what is interpreted as two different spinel phases, an aluminous- and a ferrite-rich spinel. One analysis of TKC spinel in the field that is marked as a ‘spinel not stable’ (Fig. 10c) is believed to overlap the boundary between an aluminous-rich and a ferric-iron-rich spinel.

The spinel in the Igwisi Hills samples has three major zones (Fig. 11); a core of chromite (Chr) surrounded by magnesio-ulvöspinel-magnetite (Mum) with an outer rim of aluminous pleonaste spinel (Ple). The Chr and Mum spinel boundary could not be distinguished by BSE imaging, but was easily distinguished by X-ray (Fe, Ti, Cr)

mapping (not shown). This sharp boundary is parallel to the crystal outline and has been accentuated by continuous lines in Fig. 11d and e. In contrast, the Mum–Ple boundary is easily distinguished by BSE imaging (Fig. 11d and e) because of the large difference in average atomic number. The spinel zoning trend from Mum to Ple, as shown by the bold arrows, is opposite to the trend Ple to Mum shown by the TKC spinel (Fig. 10). The TKC zoning trend is similar to that reported by O’Brien & Tyni (1999) for spinel in a Finnish kimberlite and the Igwisi trend is similar to that reported by Pasteris (1980) for spinel found in DeBeers kimberlite that is adjacent to the contact with the host rock.

The Iron Mt. kimberlite contains atoll spinel that tends to be concentrated in certain areas of the thin section. The so-called lagoon between the core and the rim (Fig. 12d and e) is mainly filled with unknown material that is high in Si, Ca, Fe and Ti and has an analytical total usually below 90 wt %, which suggests a hydrous phase. An attempt to identify this material by localized X-ray diffraction was not successful. The composition of the core spinel of most atolls is in field Chr whereas that of the rim lies in field Mum. It is very difficult, however, to analyze the narrow rims of atolls without including elements in the surrounding material. Commonly the lagoon extends around only part of the crystal (e.g. point n in Fig. 12e).

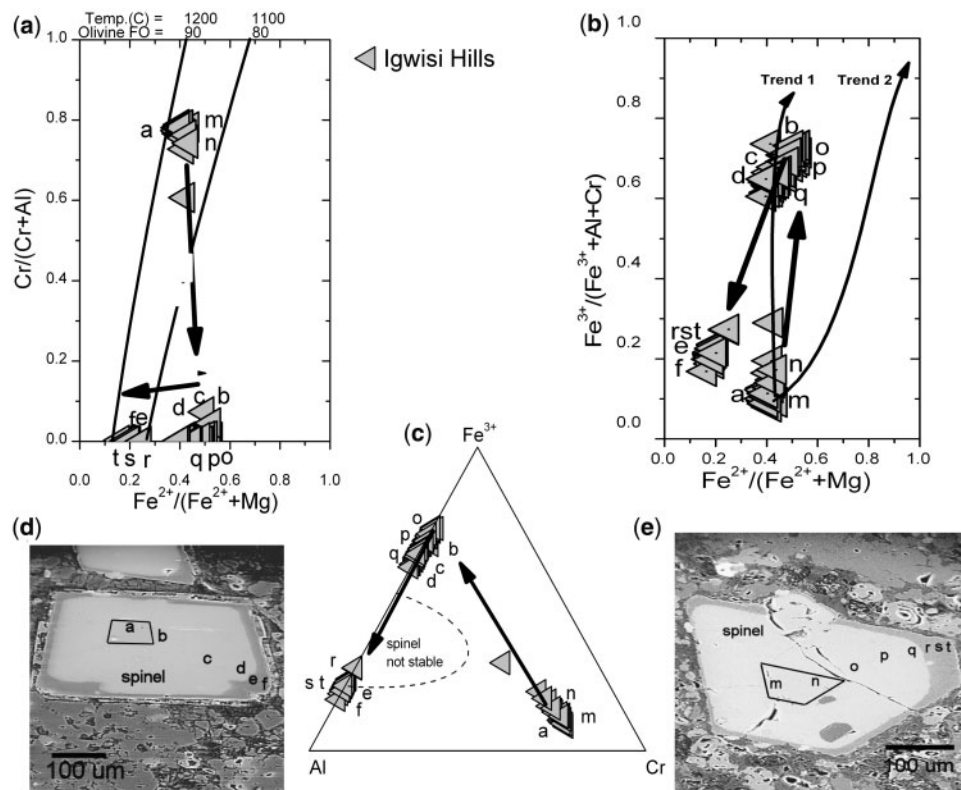


**Fig. 11.** (a–c) Three projections of oxidized spinel prism for Igwisi Hills spinel. Arrows indicate direction of zoning. (d, e) BSE images. Continuous lines have been added to differentiate the core Chr from the Mum spinel as found by X-ray mapping.

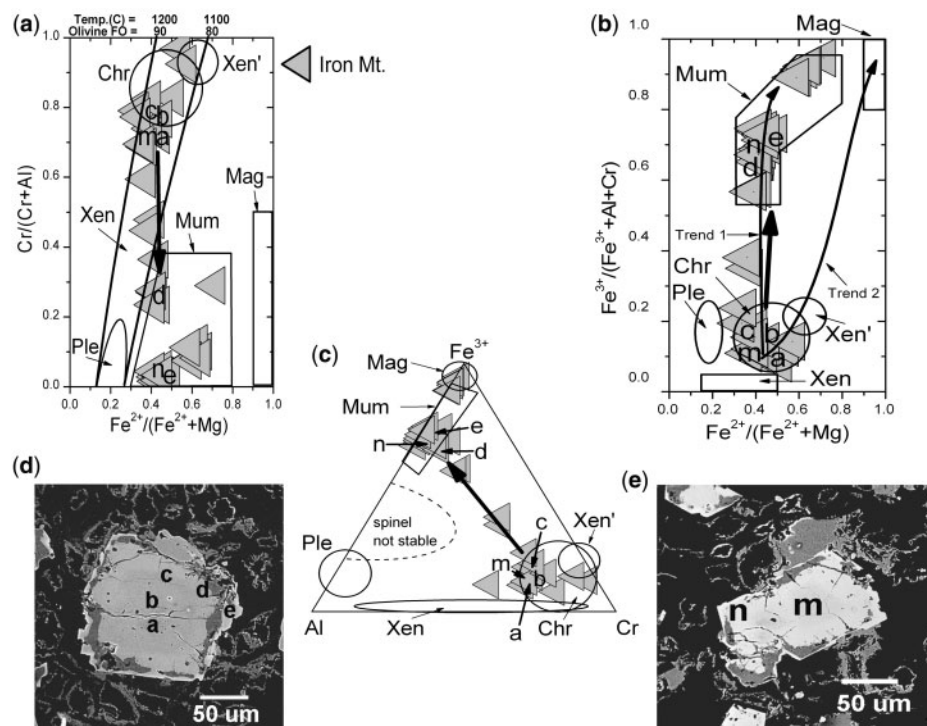


**Fig. 12.** (a–c) Three projections of oxidized spinel prism for Iron Mt. spinel. Arrow indicates direction of zoning in atoll spinel. (d, e) BSE images of atoll spinel.

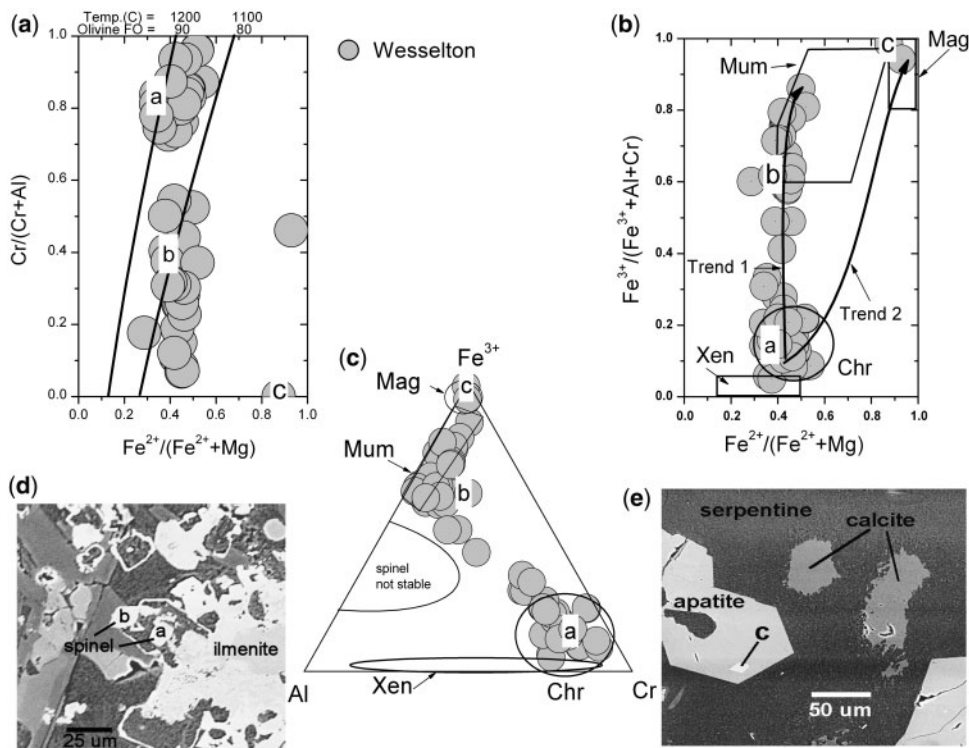


**Fig. 13.** (a–c) Three projections of oxidized spinel prism for the Wesselton kimberlite intrusions (W-2, W-3, W-5, W-8), as identified by Shee (1985). (d, e) BSE images.

The composition of spinel from four of the Wesselton (Shee, 1984) kimberlite intrusions (W-2, W-3, W-5, W-6) is shown in Fig. 13. The spinel shows a typical Trend 1 with a fairly narrow range of  $\text{Fe}^{2+}/(\text{Fe}^{2+} + \text{Mg})$ , which is consistent with that reported by Shee (1984). Shee (1984, 1985) showed consistent differences in  $\text{Fe}^{2+}/(\text{Fe}^{2+} + \text{Mg})$  of spinel between different phases with  $\text{Fe}^{2+}/(\text{Fe}^{2+} + \text{Mg})$  being highest within a sill and  $\text{Fe}^{2+}/(\text{Fe}^{2+} + \text{Mg})$  being lowest for phase W-8. There are many xenocrysts of ilmenite (Fig. 13d) that have a complex reaction rim of perovskite and spinel. Spinel a is in field Chr, which is consistent with an early primary spinel, and spinel b is in field Mum. Spinel c (Fig. 13e) is enclosed in a euhedral crystal of apatite within a segregation of serpentine and calcite. This spinel is almost pure magnetite and has a composition that is consistent with having crystallized at a very late stage.

The Benfontein Sill has many mineralogical and chemical characteristics that are typical of kimberlite as reported by Dawson & Hawthorne (1973). The sample used in the present study is dominated by relatively large spinel octahedra within a matrix of calcite and dolomite. The spinel has two very distinctive compositions, which are shown in Fig. 14. Two small euhedral spinel grains enclosed within a serpentinized olivine phenocryst with euhedral outlines are shown in Fig. 14d. These spinel grains are similar to

primary spinel (Chr) that have been described for other kimberlites (Figs 6–13). The majority of the spinel crystals are significantly larger euhedral octahedra with a reaction rim that is composed of Fe-rich chlorite (Fig. 14e). The composition of these larger spinel grains falls well within the Mum field and shows little chemical variation. The two major populations of spinel in this sample are magnesian-rich with the same  $\text{Fe}^{2+}/(\text{Fe}^{2+} + \text{Mg})$  and thus are consistent with Trend 1, as are the published Benfontein spinel analyses (Dawson & Hawthorne, 1973; Boctor & Boyd, 1981; McMahon & Haggerty, 1984).

## DISCUSSION

### Comparison of spinel in kimberlite and basaltic rocks

The majority of previously published kimberlitic spinel analyses (Fig. 1) and analyses from the present study (Fig. 4a) plot in the Chr and Mum fields. This suggests that the spinel analyses in these two fields represent two significant stages of growth in the crystallization of kimberlite. It is probable that some analyses that fall between the Chr and Mum fields are due to the analyst not being able to distinguish different zones because of their similar BSE contrast.

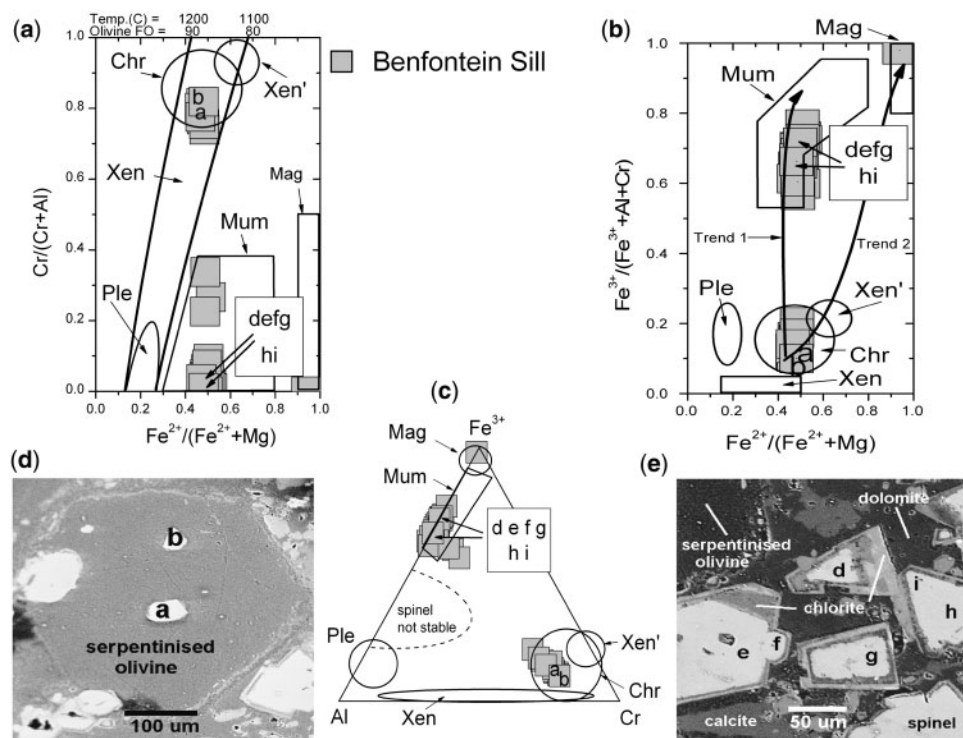


**Fig. 14.** (a–c) Three projections of oxidized spinel prism for Benfontein Sill spinel. (d, e) BSE images.

It is instructive to compare the analyses of spinel found in kimberlite with those of spinel found in basaltic volcanic rocks. The three projections of the oxidized spinel prism are shown for spinel in kimberlite (Fig. 15a, c, e) of the present study and for published spinel analyses of basaltic rocks (Fig. 15b, d, f) from the spinel database of Barnes & Roeder (2001). The two major fields 'Primary spinel' and 'Magnetite' have been identified for the basaltic spinel to emphasize the differences and similarities compared with the two fields Chr and Mum of kimberlitic spinel (Fig. 15a, c, e). The two olivine–spinel iso-potential lines are included in Fig. 15a for comparative purposes. The primary Chr spinel in kimberlite has a high  $\text{Cr}/(\text{Cr} + \text{Al})$  of 0.75–0.95 whereas the primary chromite and chromian spinel of basaltic volcanic rocks span a large range of  $\text{Cr}/(\text{Cr} + \text{Al})$  of 0.2–0.9 because the basalts range in composition from MORB to boninites (Roeder *et al.*, 2001). The  $\text{Fe}^{2+}/(\text{Fe}^{2+} + \text{Mg})$  values for primary chromite are similar for kimberlite and basaltic spinel. A very distinctive difference (Fig. 15c and d) between basaltic and kimberlitic spinel is the concentration of analyses in the Mum field and Magnetite field. The majority of the kimberlitic spinel analyses are more magnesian [lower  $\text{Fe}^{2+}/(\text{Fe}^{2+} + \text{Mg})$  at high values of  $\text{Fe}^{3+}$ ] and follow Trend 1 whereas the majority of the basaltic spinel analyses follow a trend [higher  $\text{Fe}^{2+}/(\text{Fe}^{2+} + \text{Mg})$ ] similar to Trend 2 of kimberlite.

One of the interesting similarities between the kimberlitic (Fig. 15c) and basaltic spinel (Fig. 15d) is the lower number of analyses between what we would term primary spinel (low  $\text{Fe}^{3+}$ ) and late spinel (high  $\text{Fe}^{3+}$ ). We believe this paucity of analyses for the basaltic spinel is partly due to the reaction relationship between early Cr-rich spinel and melt to produce clinopyroxene (Irvine, 1967; Hill & Roeder, 1974). However, this gap in spinel analyses for both kimberlite and basaltic spinel may in part be due to the cooling conditions and to the choice of samples both for analysis and publication by researchers.

### Major stages of spinel growth and zoning in kimberlites

Figures 16 and 17 are schematic diagrams that are designed to emphasize the major stages of spinel growth found in kimberlites (Xen, Chr, Mum, Ple, Mag) and the principal trends (1–8) of spinel zoning (arrows). Some of the major stages of spinel growth and zoning trends for single kimberlites have been previously identified (i.e. Mitchell, 1986, 1995) but the present study is the first to publish a large number of groundmass spinel analyses from a number of kimberlites to better compare the various stages and zoning trends. The present study is also the first to compare in detail the zoning trends in kimberlite groundmass spinel with the common zoning trends found in basaltic glasses.

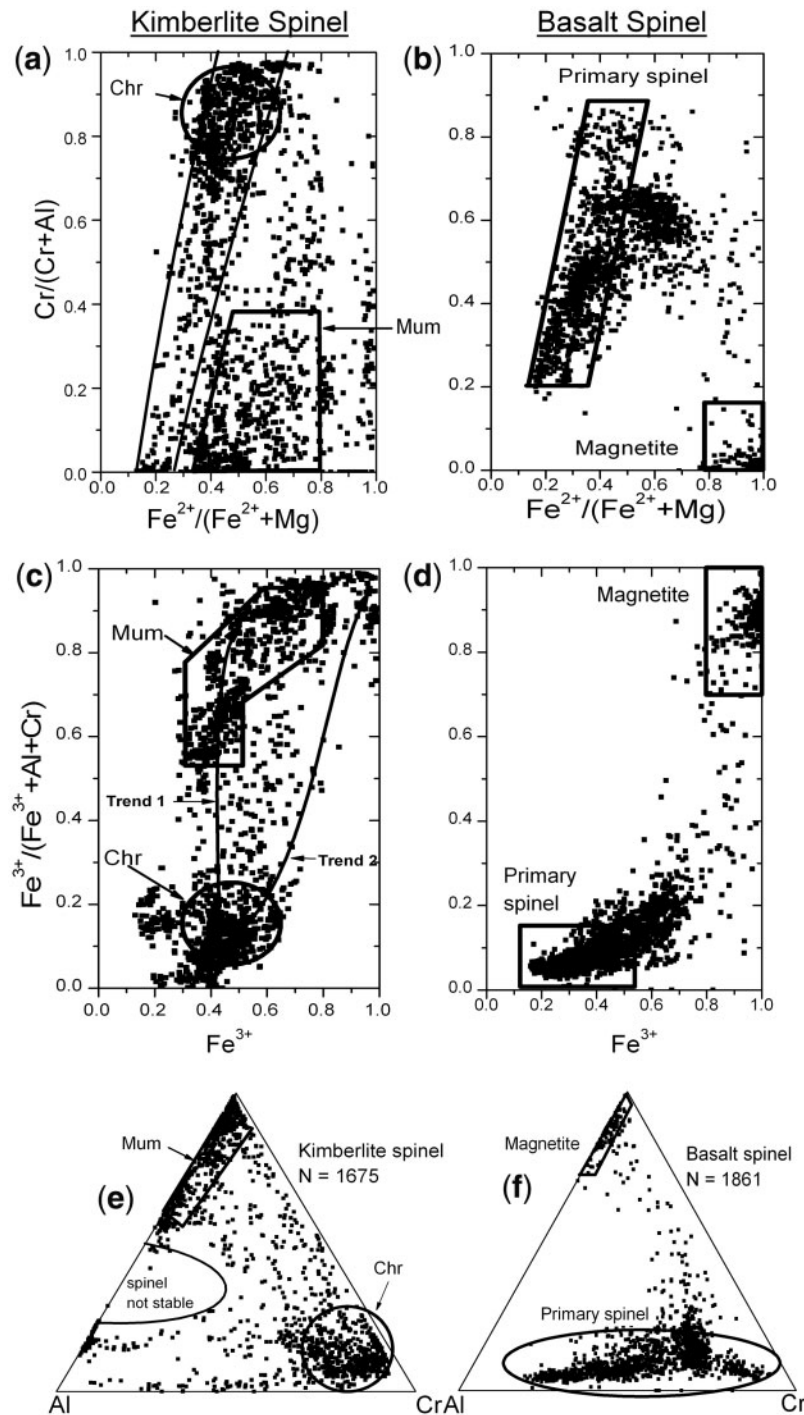


**Fig. 15.** (a, c, e) Three projections of oxidized spinel prism for kimberlite spinel of present study. (b, d, f) Three projections of oxidized spinel prism for basaltic spinel from database described by Barnes & Roeder (2001). The basaltic spinel are in samples that include boninite, alkali basalt and MORB.

The earliest spinel grains are xenocrysts (Xen, Xen') that crystallized in peridotite in the upper mantle. These xenocrysts were derived by fragmentation of peridotite either during inclusion in the kimberlitic magma or during the journey towards the Earth's surface. After

fragmentation the surfaces of the spinel xenocrysts that were exposed to kimberlitic magma were overgrown by primary spinel (Chr) or have reaction zones around the xenocrysts as indicated by zoning Trends 4 and 5 (Figs 16 and 17). The majority of the Chr spinel grains are thought

to be primary chromite that crystallized directly from the kimberlitic magma. These chromite grains are usually small in size and are thought to have been euhedral octahedra (e.g. central zone in Fig. 11d and e) that were later overgrown by the much larger volume of Mum spinel. We believe that the discrete Chr chromite is analogous to the small euhedral chromite and chromian spinel octahedra found in many rapidly cooled basalts. Roeder *et al.* (2006) demonstrated that basaltic magma may have only a small

volume per cent (<0.1 vol. %) of such spinel, but that it may be dispersed as a suspension of tens of thousands to hundreds of thousands of tiny spinel crystals per cubic centimetre of melt. The early co-crystallization of olivine and spinel in many basalts (Roeder *et al.*, 2006) and kimberlites (Mitchell, 2006, 2008) may reflect decreasing pressure during passage of the magma towards the Earth's surface.

The principal spinel zoning trend that follows the crystallization of primary Chr in kimberlite is Trend 1, and to a lesser extent Trends 2 and 3. The different spinel trends can be explained by differences in cooling rate and some combination of four basic factors.

#### *Effect of spinel immiscibility on spinel zoning trends*

Spinel solid solution is interrupted by solid immiscibility (Mitchell, 1986), the extent of which depends upon temperature of crystallization and the spinel composition. Sack & Ghiorso (1991) presented diagrams showing the extent of spinel solid solution in equilibrium with olivine at various temperatures as calculated from thermodynamic data. It is not possible to use these diagrams in a quantitative sense but they help us to understand spinel immiscibility in a qualitative sense. Sack & Ghiorso (1991) demonstrated that there is immiscibility between the aluminate and ferrite spinel at all temperatures of kimberlite crystallization (<1200°C) whereas there is miscibility between chromite and ferrite spinel at higher temperatures but possible immiscibility as temperatures approach 600°C. Figure 16 is drawn to be consistent with the general sense of the Sack & Ghiorso (1991) diagrams and to show

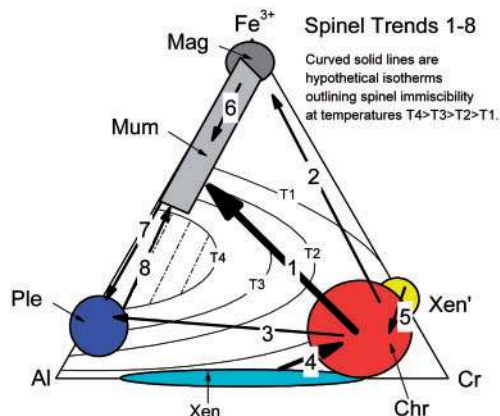


**Fig. 16.** Ternary Al–Cr–Fe<sup>3+</sup> diagram showing the major spinel Xen, Xen', Chr, Mum, Ple, Mag fields in different colours and the zoning Trends 1–8 by arrows (line-weight proportional to abundance of trends as found in present study). The curved lines T1 to T4 represent hypothetical isotherms of the spinel solvus with temperatures T4 > T3 > T2 > T1.

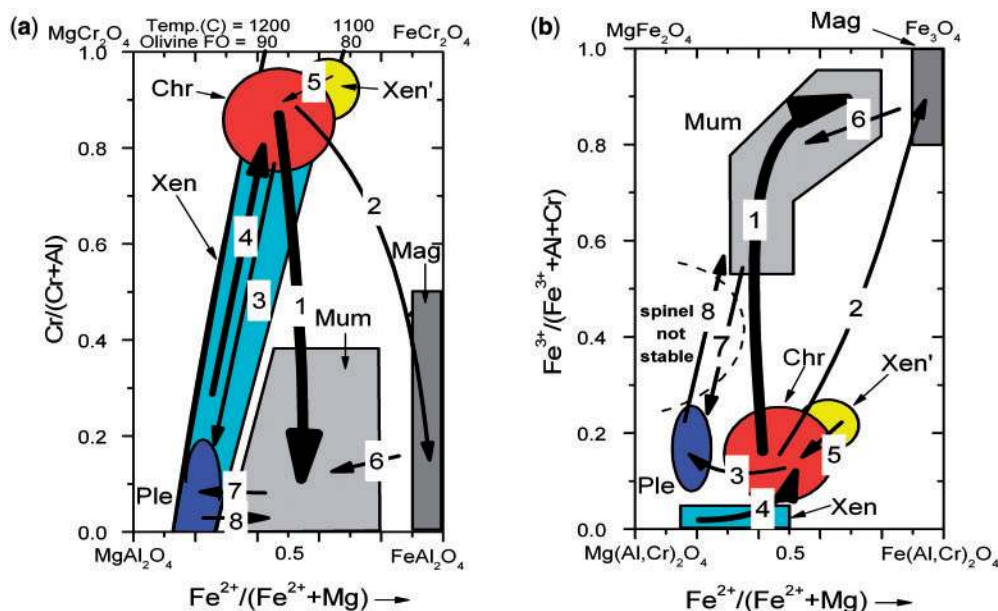


**Fig. 17.** Diagrams showing the major spinel Xen, Xen', Chr, Mum, Ple, Mag fields in colour and the zoning Trends 1–8 by arrows (line weight proportional to abundance of trends as found in present study). (a) Cr/(Cr+Al) vs Fe<sup>2+</sup>/(Fe<sup>2+</sup>+Mg). (b) Fe<sup>3+</sup>/(Fe<sup>3+</sup>+Al+Cr) vs Fe<sup>2+</sup>/(Fe<sup>2+</sup>+Mg).

how the extent of spinel solid solution may vary as a function of the hypothetical solvus temperatures of T1 to T4. No attempt has been made to show how the variation in  $\text{Fe}^{2+}/(\text{Fe}^{2+} + \text{Mg})$  and Ti would affect these hypothetical solvus isotherms. The limited miscibility between aluminate and ferrite spinel can be seen by the few analyses of kimberlitic and basaltic spinel near the Al–Fe<sup>3+</sup> join in Fig. 15e and f.

The first spinel (Chr) that crystallizes from kimberlite magma is very high in chromium and has a composition near the Cr apex in Fig. 16. The crystallization of primary spinel produces zoning Trends 1, 2 and 3 all directly away from the Cr apex. The aluminous Trend 3 is drawn to be consistent with the zoning of the TKC spinel (Fig. 10) and the unique crystal in the New Elands sample (Fig. 9). If the hypothetical isotherms in Fig. 16 are correct, Trend 2 is least likely to intersect the spinel solvus. The aluminous Trends 7 and 8 are most likely to intersect the spinel solvus as the spinel changes from Chr to Ple to Mum or from Chr to Mum to Ple. We believe that the TKC (Fig. 10) and the Igwisi (Fig. 11) spinel are examples where the spinel solvus was intersected, as shown by the abrupt change in electron back-scattering at the Ple–Mum interface. The TKC spinel often has Ple as rims on Chr whereas the Mum often occurs as separate grains in the ground-mass. The BSE image of the unique New Elands crystal (Fig. 9e) shows a discrete boundary between the c and d zones and a lagoon in the lower part of the crystal. It may be that the spinel solvus was intersected by this spinel, or the solvus influenced the lack of growth of spinel d on the planar faces. We suggest that the New Elands crystal (Fig. 9e) was free to grow downwards at the corners (d), but lack of spinel constituents in the melt close to the growing crystal face, and/or spinel immiscibility, caused formation of the lagoon. The change of c to d in Fig. 9c is parallel to Trend 8 in Fig. 16.

Pasteris (1980) and Mitchell (1986, 2006, 2008) have suggested that the so-called lagoons found in atoll spinel were produced by a reaction that removed previously formed aluminous spinel. If the spinel solvus had some influence on the crystallization trends we would predict that Trend 1 would be more influenced than Trend 2, as shown (Fig. 16) by the position of these two trends relative to the suggested solvus temperatures (T1 to T4). This may be the reason why atolls are more likely to be found in Group I kimberlites where spinel tends to follow Trend 1. Armstrong *et al.* (1997) suggested that atoll formation was caused by supersaturation and rapid cruciform growth of spinel at the corners of the crystal whereas the faces of the crystal did not have enough spinel constituents nearby to complete the face. Mitchell (1986) noted that the most common phases between the atoll core and rim are serpentine and carbonate. We have confirmed this observation and also observed an unidentified phase (Fig. 12d and e)

in the lagoon in some kimberlites (e.g. Iron Mt.). We suggest that the lagoon represents a volume where spinel never crystallized, because of lack of spinel constituents and/or spinel immiscibility. This volume could at that stage have been the oxide–silicate kimberlite melt or a separate immiscible fluid phase.

### *Rapid growth of spinel*

Rapid thermal fluctuations in a kimberlitic or basaltic magma may cause rapid growth of spinel and thus locally deplete spinel constituents ahead of the growing crystal (Roeder *et al.*, 2001). Both kimberlitic and basaltic spinel can display significant zoning from high-Cr to high-Al spinel parallel to the olivine–spinel iso-potential lines (Trend 3).

The Trend 3 spinel zoning for two kimberlites [TKC and Finnish kimberlite (O'Brien & Tyni, 1999)] are compared in Fig. 18 with zoning in two MORB spinel grains (Fig. 18d and e) from the East Pacific Rise (Roeder *et al.*, 2001). The zoning of the TKC spinel is shown by black arrows, the spinel zoning of the Finnish kimberlite (O'Brien & Tyni, 1999) by yellow arrows and the spinel zoning in the MORB spinel by the blue arrows. Natland (1989) described zoning in East-Pacific Rise basaltic spinel that was parallel to olivine–spinel iso-potential lines (Fig. 18a), and he ascribed it to crystallization from melts with a narrow range of  $\text{Fe}^{2+}/(\text{Fe}^{2+} + \text{Mg})$ . This type of zoning is common in basaltic samples and often results in alternating zones as seen in Fig. 18e. Roeder *et al.* (2001) explained this type of zoning by the varying rate of diffusion of Cr in the melt ahead of a rapidly growing crystal at near constant  $\text{Fe}^{2+}/(\text{Fe}^{2+} + \text{Mg})$  in the melt. We believe that the spinel Trend 3 (Chr to Ple) for the two kimberlites and the MORB sample shown in Fig. 18 result from the same process of rapid growth at a high degree of supersaturation of spinel. The extent of the Cr/(Cr + Al) zoning is much greater for the two kimberlite samples than for all the basalt samples described by Roeder *et al.* (2001). This may in part be due to a significantly lower viscosity of kimberlitic melt and/or more rapid thermal changes in kimberlite melt. The extent of these thermal changes is unknown.

Grutter & Apter (1998, fig. 7) showed an example in kimberlite of a low-TiO<sub>2</sub> xenocrystic chromite surrounded by a vermiciform rim. They ascribed the vermiciform rim as due to crystallization 'within an ascending saturated kimberlite or lamproite magma'. A very similar texture was found by Roeder *et al.* (2001) in a high-temperature experiment on a MORB glass and was ascribed to crystallization, not resorption.

Most of the kimberlitic spinel examined in the present study shows marked changes in composition over very small distances, which suggests rapidly changing conditions at stages Chr, Mum and Ple with little or no spinel homogenization at a later time. An obvious exception is the large euhedral spinel grains in the Benfontein Sill that

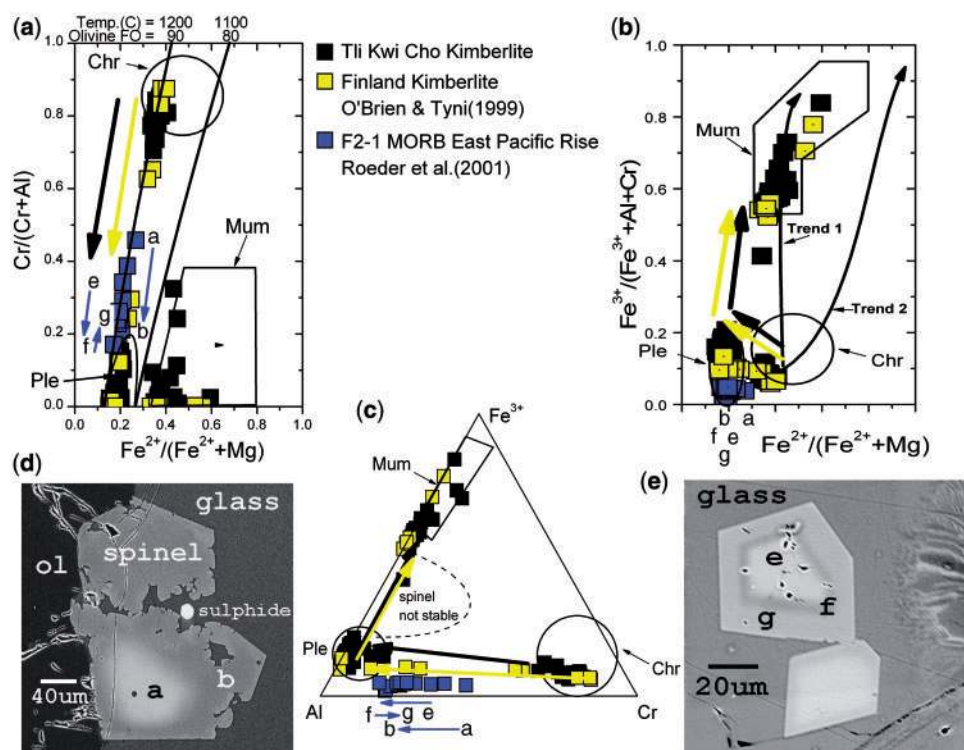


**Fig. 18.** (a–c) Three projections of oxidized spinel prism for the spinel analyses (black) of the Tli Kwi Cho kimberlite, spinel analyses (yellow) of Finland kimberlites published by O'Brien & Tyni (1999) and spinel analyses (blue) of the F2-1 MORB of the East-Pacific Rise published by Roeder *et al.* (2001). Lines with arrows show zoning trends. Lower-case letters indicate analyses for points on the BSE images. (d, e) BSE images of spinel in basaltic glass (sample F2-1).

are unzoned, which suggests relatively slow crystallization or at least a long period of time at temperatures high enough to promote homogenization of the spinel, as might be expected in the relatively slower-cooling environment of a sill.

#### *Significant differences in melt composition*

An obvious factor that can influence spinel compositional trends is the difference in composition of different batches of kimberlitic magma. We know little about the original composition of kimberlitic magma because late processes have often destroyed evidence of the original melt composition. There are obvious differences in the  $\text{Fe}^{2+}/(\text{Fe}^{2+} + \text{Mg})$  of primary (Chr) spinel in different kimberlites such as shown by the Ekati, Jericho and Rich kimberlites (Fig. 7) and in kimberlites described by Pasteris (1980), Shee (1985), Mitchell (1986) and Masun (1999). There is evidence that very small differences in the  $\text{Fe}^{2+}/(\text{Fe}^{2+} + \text{Mg})$  of primary Chr may be followed by larger differences in later spinel as shown by the differences of Trends 1 and 2 for the Grizzly and Rich spinel (Fig. 6a). The crystallization of early phlogopite in Group II kimberlite has often been cited (i.e. Pasteris, 1980; Mitchell, 1986) as the primary reason for Mg and Al decreasing in the melt and thus increasing the  $\text{Fe}^{2+}/(\text{Fe}^{2+} + \text{Mg})$  as shown for

Trend 2 spinel. We agree with the proposition of Pasteris (1980) that lack of phlogopite crystallization may have been responsible for spinel zoning demonstrated by Trend 7 from Mum to Ple spinel for the Igwisi Hills samples (Fig. 11), and also reported by Reid *et al.* (1975) and Dawson (1994).

There are significant differences in the amount of carbonate associated with kimberlites containing Trends 1 and 2 spinel. One of the characteristics of many Group I kimberlites is the presence of carbonate segregations that formed late in the crystallization history of the kimberlite. It has been noted by many researchers (e.g. Mitchell, 1986; Armstrong *et al.*, 2004) that carbon dioxide and water are very important components in the late evolution of kimberlite. It has been suggested that the evolution of these volatile components for some kimberlites may be almost explosive because of depressurization of the kimberlitic magma during rapid intrusion into the upper crust (Scott Smith, 1999). If the carbonate segregations represent a volume that was filled by a late vapour or an immiscible fluid phase, the minerals now in that volume may be due to crystallization of that fluid, the late infilling of that volume by intra-crystalline melt, and/or late reaction with meteoric water. The large change from stage Chr to stage Mum spinel (Fig. 11d and e) may in some cases be related

to rapid vesiculation, which in turn led to rapid changes in temperature and melt composition.

It is suggested that in those kimberlites in which carbonate played a major role the activity of magnesium remained high under relatively oxidizing conditions, thus leading to the essentially constant, and relatively low,  $\text{Fe}^{2+}/(\text{Fe}^{2+} + \text{Mg})$  of Trend 1 spinel. Some of the best examples of Trend 1 spinel were found in the Iron Mountain, Igwisi Hills, Wesselton, Udachnaya, Benfontein and the Grizzly samples. All of these samples contain either carbonate segregations or significant carbonate in the groundmass (Benfontein). Even though the Rich kimberlite is a Group I kimberlite, the spinel displays Trend 2 spinel (Crawford, 2003, and present study). However, the outermost rim of the Rich spinel (Fig. 7b) exhibits characteristics of Trend 1 spinel and it is suggested that only at a very late stage did the carbonate activity for this kimberlite have a significant influence on the spinel composition (Trend 6). However, some of the phases present today may have been very different before late reaction with meteoric water. For example, water-soluble halides and alkali carbonates found in the deeper levels of the Udachnaya-East diamondiferous pipe (Kamenetsky *et al.*, 2004, 2008; Kamenetsky, 2005; Maas *et al.*, 2005) may have been precursors to the Ca–Mg carbonates and serpentine found in the higher levels of the Udachnaya-East pipe. This may be true for other Group I kimberlites. There is evidence (Fig. 1) that spinel associated with carbonatites (Mariano & Roeder, 1983; Gaspar & Wyllie, 1984; Treiman & Essene, 1984; Barnes & Roeder, 2001; Armstrong *et al.*, 2004) or lamprophyres (Rock, 1986; Ulrych *et al.*, 1986; Tappe *et al.*, 2006) tends to have a higher amount of the magnesioferrite molecule ( $\text{MgFe}^{3+}_2\text{O}_4$ ). This is consistent with kimberlite spinel that approaches Trend 1.

#### *Spinel zoning influenced by local nucleation of other phases*

The majority of spinel in hypabyssal kimberlite crystallized very rapidly to produce zoning over a short distance and most of that spinel never homogenized. There is textural and compositional evidence that the nucleation, or lack of nucleation, of other minerals can influence the composition of spinel. For example, the majority of the spinel grains in the New Elands kimberlite follow a trend close to Trend 2 (black dots in Fig. 9a–c) and may be explained by the crystallization of phlogopite that depleted the melt in Mg and Al. However, a unique New Elands spinel crystal is thought to have been prevented from growing upwards (Fig. 9e) because of the presence of a large phlogopite crystal whereas the lower part of the spinel crystal continued to grow because no phlogopite had nucleated at that location, and thus the spinel became very aluminous.

The nucleation, or lack of nucleation of other minerals can influence not only the morphology but also the composition of nearby spinel. Many spinel grains are preserved from later reaction with the melt by the nucleation of

phases (e.g. olivine and phlogopite) that enclose the spinel (e.g. Chr in Benfontein olivine, Fig. 14b).

## CONCLUSIONS

The dramatic changes in spinel composition seen in many kimberlites have been explained by some researchers as an indication of changes in the general kimberlite melt composition, and may be useful in understanding kimberlite evolution and possibly even the conditions that control diamond preservation. The present study is based on 1675 spinel analyses from 46 samples of kimberlite and related rocks. The principal conclusions of the present study are that the morphological and compositional diversity of spinel in a single kimberlite is the result of rapidly changing thermal and pressure conditions.

The main stages of spinel growth and trends in zoning found in the present study are shown schematically in Figs 16 and 17. Each of Trends 1–8 has been found in more than one kimberlite (in the present or published studies) and an understanding of the processes that produced each of these trends reveals important information about the crystallization history of the kimberlite. Fields Xen and Xen' represent spinel xenocrysts derived from peridotite xenoliths that were swept up by kimberlitic magma as it traveled towards the Earth's surface. Those spinel xenocrysts exposed to kimberlite melt are often enclosed by primary spinel (Chr) giving zoning Trends 4 and 5. The primary spinel that first crystallizes from kimberlitic magma is thought to be small (25–100  $\mu\text{m}$ ) euhedral octahedra of high  $\text{Cr}/(\text{Cr} + \text{Al})$  chromite (Chr). It is believed that the majority of primary spinel (Chr) crystallized between the source of the kimberlitic magma in the upper mantle and the Earth's surface (Mitchell, 2006, 2008), and these tiny spinel grains may have been close to equilibrium with the kimberlitic magma. These spinel grains acted as nuclei for the zoning Trends 1, 2 and 3 that end with very low chromium spinel (Mum, Ple, Mag). We believe the Trend 3 aluminous zoning parallel to the olivine–spinel iso-potential curves of Irvine (1965) is the result of rapid thermal changes and diffusion-controlled crystallization. A similar trend is found in basaltic spinel (Roeder *et al.*, 2001). However, the  $\text{Cr}/(\text{Cr} + \text{Al})$  zoning found in two kimberlite examples, TKC and Finland (O'Brien & Tyni, 1999), is much more extensive than any reported for basaltic spinel (Roeder *et al.*, 2001). These differences in magnitude of zoning may be due to a lower melt viscosity, or more rapidly changing thermal conditions of kimberlite magma than for basaltic magma.

The majority of the zoning of spinel in kimberlites is Trend 1 from Chr to Mum (Mitchell, 1986). We believe this zoning is a result of a combination of variables that were initiated by the rapid depressurization of the kimberlite magma, which initiated evolution of carbon dioxide, rapid thermal changes and crystallization of other

groundmass minerals. It is also probable that spinel immiscibility (Figs 16 and 17b) played a role in the Trend 1 zoning. We believe carbon dioxide, or carbonate, played a prominent role in oxidizing ferrous iron and keeping the magnesium activity relatively high. No attempt was made in the present study to calculate the oxygen fugacity from the composition of spinel and coexisting olivine (Fedortchouk & Canil, 2004) because of the many assumptions that would be necessary, such as equilibrium of zoned spinel.

We examined spinel in nine Group II kimberlites and found Trend 2 spinel in only four of them (Lace, New Elands, Newlands, Roberts Victor). Thus we were unable to confirm a correlation of Trend 1 and 2 spinel with Groups I and II kimberlites respectively as suggested by Mitchell (1986). However, we agree with Pasteris (1980) and Mitchell (1986) that the crystallization of phlogopite, and other magnesian minerals, probably played a major role in changing the magma composition that resulted in Trend 2 spinel. We suggest that Trend 6 as seen in the Rich spinel may indicate the importance of carbonate in maintaining elevated magnesioferrite in spinel that is characteristic of Trend 1.

There are many analogies between the spinel found in kimberlite and in basaltic volcanic rock. The early primary crystals in kimberlites and basaltic rocks are small (<100 µm) euhedral octahedra and it is probable that the magma contained many thousands of crystals per cubic centimetre of magma (Roeder *et al.*, 2006). The primary spinel in both kimberlite and basaltic magmas is zoned from high chromium to very low chromium over a short distance because of the rapid growth and the very low solubility of chromium in silicate melts. Some of the early crystals in both kimberlitic and basaltic spinel show the aluminous Trend 3, which we ascribe to very rapid thermal changes. The major difference between the spinel zoning trends in basaltic rocks and kimberlite is the predominance of Trend 1 spinel in kimberlites. Another obvious difference is that the presence of atoll spinel seems to be restricted to kimberlite, although Roeder *et al.* (2001) found a variety of spinel crystal forms in rapidly cooled MORB that are thought to have been the result of diffusion-controlled crystallization. We thus believe that atoll spinel is a growth feature and not a result of resorption as described by Mitchell & Clark (1976) and Pasteris (1980). Because of the textural complexity of the kimberlite groundmass it was not possible to evaluate the relative volume of the spinel phases. However, the much smaller amount of Chr relative to Mum spinel is illustrated for the Igwisi samples (Fig. 11d and e). It was much more difficult to find Chr as compared with Mum spinel in the polished thin sections because of the much smaller volume of Chr present in the samples; however, Cr-rich spinel was found in all but four samples. We conclude that the smaller volume of Chr relative to

Mum is a growth feature and not a result of extensive resorption of Chr as discussed by Mitchell (1986).

The present study was undertaken with the goal of using the complex zoning in kimberlitic spinel to better understand the evolution of kimberlitic magma and the conditions that may favor diamond survivability in that magma. What we have learned is that the complex zoning in spinel is due to a combination of factors that are mainly the result of rapidly changing conditions that were far from equilibrium. These rapidly changing conditions led to local conditions such as the patchy distribution of atolls and heterogeneous nucleation of phases that sometimes influenced the composition of spinel. It is possible that the spinel zoning trends may with further study be useful in estimating the rate of change of conditions for kimberlite magma. An attempt was made in the present study to correlate spinel composition and spinel zoning trends with the diamond content of single kimberlites. However, no obvious correlation was found such as that described (Van Straaten *et al.*, 2006) for the Victor Northwest Kimberlite Pipe.

## SUPPLEMENTARY DATA

Supplementary data for this paper are available at *Journal of Petrology* online.

## ACKNOWLEDGEMENTS

The following individuals and organizations provided materials, logistical or other assistance that aided in collection of samples used in this study: De Beers, Lac Minerals, Cominco, Diamond Company, Guanimo Mining Company, Barry Hawthorne, Mike Skinner, Roger Clement, John Bristow, Alex Van Zyl, Leonard Kleinjen, Jock Robey, Fanus Viljoen, Mike McGurl, George Read, David Bell, Stephan Kurszlaukis, Bruce Wyatt, Don Boucher, Herman Grutter, Casey Hetman, Adrian Van Rythoven, Barry Dawson, John Gurney, Rory Moore, Joe Brummer, Chris Pegg, Herb Helmstaedt, Howard Coopersmith, Mal McCallum, Dave Egger, Chris Jennings, Bruce Kjarsgaard, Carter Hearn, Keith Barron, Mark Badham, Robert Cooper, Dominic Channer, Patrick Anderson, Jim Crawford, Maya Kopylova, Robert Cassie, Susan Kay, Brian Paniatowsky and Victoria Yehl. This study would not have been possible without their help, which we gratefully acknowledge. Tom Nowicki and Herman Grutter are thanked for providing constructive comments and suggestions on an early version of the manuscript. David Phillips, Bruce Wyatt, Nick Sobolev, Majorie Wilson and Alastair Lumsden are thanked for their very constructive comments and review of the manuscript. We also acknowledge the pioneering studies on the mineralogy and petrology of kimberlites by Joe Boyd, Barry Dawson, Steve Haggerty, Roger Mitchell and Jill Pasteris. Joan Charbonneau, David Kempson and Jerzy Adwent are thanked for their technical support.

Financial support was provided by the Natural Sciences and Engineering Research Council of Canada.

## REFERENCES

- Agee, J. J., Garrison, J. R. & Taylor, L. A. (1982). Petrogenesis of oxide minerals in kimberlite, Elliott County, Kentucky. *American Mineralogist* **67**, 28–42.
- Allsopp, H. L., Bristow, J. W. & Skinner, E. M. W. (1985). The Rb–Sr geochronology of the Colossus kimberlite pipe, Zimbabwe. *South African Journal of Geology* **88**(2), 245–248.
- Arima, M. & Kerrich, R. (1988). Jurassic kimberlites from Picton and Varty Lake, Ontario: Geochemical and stable isotopic characteristics. *Contributions to Mineralogy and Petrology* **99**(3), 385–391.
- Armstrong, J. P., Wilson, M., Barnett, N. L., Nowicki, T. & Kjarsgaard, B. A. (2004). Mineralogy of primary carbonate-bearing hypabyssal kimberlite, Lac de Gras, Slave Province, Northwest Territories, Canada. In: Mitchell, R. H., Grutter, H. S., Heaman, L. M., Scott Smith, B. H. & Stachel, T. (eds) *8th International Kimberlite Conference Proceedings*. Amsterdam: Elsevier, pp. 415–433.
- Armstrong, K. A., Roeder, P. L. & Helmstaedt, H. H. (1997). Composition of spinels in the C14 kimberlite, Kirkland Lake, Ontario. *Russian Geology and Geophysics* **38**(2), 454–466.
- Barnes, S. J. & Roeder, P. L. (2001). The range of spinel compositions in terrestrial mafic and ultramafic rocks. *Journal of Petrology* **42**, 2279–2302.
- Barron, K. M. & Barnett, R. L. (1993). A kimberlite–kamaugite transition? Kalsite-bearing kimberlite from the New Buffonta gold mine, Kirkland Lake area, northeastern Ontario. In: Dunn, K. & Grant, B. (eds) *Mid-Continent Diamonds*. Toronto, Ont.: Geological Association of Canada, pp. 37–45.
- Becker, M. & le Roex, A. P. (2006). Geochemistry of South African on- and off-craton, Group I and Group II kimberlites: Petrogenesis and source region evolution. *Journal of Petrology* **47**(4), 673–703.
- Bell, D. R. & Mofokeng, S. W. (1998). Cr-poor megacrysts from the Frank Smith Mine and the source region of transitional kimberlites. In: *Extended Abstracts of the 7th International Kimberlite Conference*. Cape Town: University of Cape Town, pp. 64–66.
- Bector, N. Z. & Boyd, F. R. (1981). Oxide minerals in a layered kimberlite–carbonate sill from Benfontein, South Africa. *Contributions to Mineralogy and Petrology* **76**, 253–259.
- Bector, N. Z. & Boyd, F. R. (1982). Petrology of kimberlites from the DeBruyn and Martin Mine, Bellsbank, South Africa. *American Mineralogist* **67**, 917–925.
- Chakhmouradian, A. R. & Mitchell, R. H. (2001). Three compositional varieties of perovskite from kimberlites of the Lac de Gras field (Northwest Territories, Canada). *Mineralogical Magazine* **65**, 133–148.
- Coopersmith, H. G., Mitchell, R. H. & Hausel, W. D. (2003). Kimberlites and lamproites of Colorado and Wyoming, USA. In: Kjarsgaard, B. A. (ed.) *Guidebook for 8th International Kimberlite Conference*. Ottawa, Ont.: Geological Survey of Canada Bookstore, 30 pp.
- Crawford, J. (2003). A comparative study of hypabyssal kimberlite from four locations within the Slave Craton of Northern Canada. M.Sc. thesis, Queen's University, Kingston, Ont.
- Dawson, J. B. (1967). A review of the geology of kimberlite. In: Wyllie, P. J. (ed.) *Ultramafic and Related Rocks*. New York: John Wiley, pp. 241–251.
- Dawson, J. B. (1994). Quaternary kimberlitic volcanism on the Tanzania craton. *Contributions to Mineralogy and Petrology* **116**, 473–485.
- Dawson, J. B. & Hawthorne, J. B. (1973). Magmatic sedimentation and carbonatitic differentiation in kimberlitic sills at Benfontein, South Africa. *Journal of the Geological Society, London* **129**, 61–85.
- Doden, A. G., Mbalu-Keswa, C. & Gold, D. P. (1998). Geology and mineralogy of the Tanoma kimberlite, SW PA: Evaluation of diamond potential. *Geological Society of America, Programs with Abstracts* **30**(1), 14–15.
- Doyle, B. J., Kivi, K. & Scott Smith, B. H. (1999). The Tli Kwi Cho. (Do27 and Do18) diamondiferous kimberlite complex, Northwest Territories, Canada. In: Gurney, J. J., Gurney, J. L., Pascoe, M. D. & Richardson, S. H. (eds) *The J. B. Dawson Volume, Proceedings of the 7th International Kimberlite Conference*. Cape Town: Red Roof Design, pp. 194–204.
- Edwards, D., Rock, N. M. S., Taylor, W. R., Griffin, B. J. & Ramsay, R. R. (1992). Mineralogy and petrology of the Aries diamondiferous kimberlite pipe, Central Kimberley Block, Western Australia. *Journal of Petrology* **33**(5), 1157–1191.
- Fedortchouk, Y. & Canil, D. (2004). Intensive variables in kimberlite magmas, Lac de Gras, Canada and implications for diamond survival. *Journal of Petrology* **45**(9), 1725–1745.
- Ford, F. D. (1987). Petrology and geochemistry of xenoliths from the Blaauwbosch kimberlite pipe. B.Sc. thesis, Queen's University, Kingston, Ont.
- Gaspar, J. C. & Wyllie, P. J. (1984). The alleged kimberlite–carbonatite relationship: evidence from ilmenite and spinel from Premier and Wesselton Mines and the Benfontein Sill, South Africa. *Contributions to Mineralogy and Petrology* **85**, 133–140.
- Grutter, H. & Apter, D. (1998). Kimberlite- and lamproite-borne chromite phenocrysts with 'diamond-inclusion'-type chemistries. In: *Extended Abstracts of the 7th International Kimberlite Conference*. Cape Town: University of Cape Town, pp. 280–282.
- Haggerty, S. E. (1975). The chemistry and genesis of opaque minerals in kimberlite. In: Ahrens, L. H., Dawson, J. B., Duncan, A. R. & Erlank, A. J. (eds) *Physics and Chemistry of the Earth*, 9. Oxford: Pergamon Press, pp. 295–307.
- Hall, D. C. (1991). A petrological investigation of the Cross kimberlite occurrence, southeastern British Columbia, Canada. Ph.D. thesis, Queen's University, Kingston, Ont.
- Hill, R. & Roeder, P. L. (1974). The crystallization of spinel from basaltic liquid as a function of oxygen fugacity. *Journal of Geology* **82**, 709–729.
- Hill, S. J. (1989). A study of the diamonds and xenoliths from the Star Kimberlite, Orange Free State, South Africa. M.Sc. thesis, University of Cape Town.
- Hunter, R. H., Kissling, R. D. & Taylor, L. A. (1984). Mid- to late-stage kimberlitic melt evolution: Phlogopites and oxides from the Fayette County kimberlite, Pennsylvania. *American Mineralogist* **69**, 30–40.
- Irvine, T. N. (1965). Chromian spinel as a petrogenetic indicator. Part I. Theory. *Canadian Journal of Earth Sciences* **2**, 648–672.
- Irvine, T. N. (1967). Chromian spinel as a petrogenetic indicator. Part 2. Petrologic implications. *Canadian Journal of Earth Sciences* **4**, 71–103.
- Jarosewich, E. J., Nelen, J. A. & Norberg, J. A. (1980). Reference samples for electron microprobe analysis. *Geostandards Newsletter* **4**, 257–258.
- Jensen, S. M. & Secher, K. (2003). Investigating the diamond potential of southern West Greenland. *Geological Survey of Denmark and Greenland Bulletin, Review of Survey Activities* **4**, 69–72.

- Kamenetsky, M. B. (2005). New identity of the kimberlite melt: Constraints from unaltered diamondiferous Udachnaya-East Pipe kimberlite, Siberia, Russia. PhD thesis, University of Tasmania, Hobart.
- Kamenetsky, M. B., Sobolev, A. V., Kamenetsky, V. S., Maas, R., Danyushevsky, L. V., Thomas, R., Pokhilenko, N. P. & Sobolev, N. V. (2004). Kimberlite melts rich in alkali chlorides and carbonates: A potent metasomatic agent in the mantle. *Geology* **32**(10), 845–848.
- Kamenetsky, V. S., Kamenetsky, M. B., Sobolev, A. V., Golovin, A. V., Demouchy, S., Faure, K., Sharygin, V. V. & Kuzmin, D. V. (2008). Olivine in the Udachnaya-East Kimberlite (Yakutia, Russia): Types, compositions and origins. *Journal of Petrology* **49**(4), 823–839.
- Kaminsky, F. V., Sablukov, S. M., Sablukova, L. I. & Channer, D. M. (2004). Neoproterozoic 'anomalous' kimberlites of Guaniamo, Venezuela: Mica kimberlites of isotopic transitional type. *Lithos* **76**, 565–590.
- Kjarsgaard, B. A. & Wyllie, R. S. J. (1993). Geology of Paul Lake area, 76D/9, Northwest Territories. Geological Survey of Canada Open File Map 2739, scale 1:50 000.
- Kurszlaukis, S. & Franz, L. (1998). Blue Hills Intrusive Complex. In: *Namibia Field Excursion Guide. 7th International Kimberlite Conference*. Cape Town, pp. 65–71.
- Lapin, A. V., Tolstov, A. V. & Vasilenko, V. B. (2007). Petrogeochemical characteristics of the kimberlites from the Middle Markha region with application to the problem of the geochemical heterogeneity of kimberlites. *Geochemistry International* **45**(12), 1197–1209.
- Maas, R., Kamenetsky, M. B., Sobolev, A. V., Kamenetsky, V. F. & Sobolev, N. V. (2005). Sr, Nd, and Pb isotope evidence for a mantle origin of alkali chlorides and carbonates in the Udachnaya kimberlite, Siberia. *Geology* **33**(7), 549–552.
- MacGregor, I. D. & Carter, J. L. (1970). The chemistry of clinopyroxenes and garnets of eclogite and peridotite xenoliths from the Roberts Victor Mine, South Africa. *Physics of the Earth and Planetary Interiors* **3**, 391–397.
- Mariano, A. N. & Roeder, P. L. (1983). Kerimasi: A neglected carbonate volcano. *Journal of Geology* **91**(4), 449–455.
- Martens, J. H. C. (1924). Igneous rocks of Ithaca, New York, and vicinity. *Geological Society of America Bulletin* **35**, 305–320.
- Masun, K. M. (1999). The petrography and mineralogy of the Lac de Gras kimberlite field, Slave Province, Northwest Territories: A comparative study. M.Sc. thesis, Lakehead University, Thunder Bay, Ont.
- McCallum, M. E. & Eggler, D. H. (1971). Mineralogy of the Sloan diatreme, a kimberlite pipe in Northern Larimer County, Colorado. *American Mineralogist* **56**, 1735–1749.
- McMahon, B. & Haggerty, S. E. (1984). The Benfontein kimberlite sills: magmatic reactions and high intrusion temperatures. *American Journal of Science* **284**, 893–941.
- Mitchell, R. H. (1979). Mineralogy of the Tunraq Kimberlite, Somerset Island, N.W.T., Canada. In: Boyd, F. R. & Meyer, H. O. A. (eds) *Kimberlites, Diatremes and Diamonds*. Washington, DC: American Geophysical Union, pp. 161–171.
- Mitchell, R. H. (1986). *Kimberlites: Mineralogy, Geochemistry and Petrology*. New York: Plenum, 442 pp.
- Mitchell, R. H. (1995). *Kimberlites, Orangeites, and Related Rocks*. New York: Plenum, 410 pp.
- Mitchell, R. H. (1997). *Kimberlites, Orangeites, Lamproites, Melilitites, and Minettes: A Petrographic Atlas*. Thunder Bay, Ont.: Almaz Press, 243 pp.
- Mitchell, R. H. (2006). Petrology of hypabyssal kimberlites. *The Kimberlite Emplacement Workshop, Saskatoon, September 2006*.
- Mitchell, R. H. (2008). Petrology of hypabyssal kimberlites: Relevance to primary magma compositions. *Journal of Volcanology and Geothermal Research* **174**(1–3), 1–8.
- Mitchell, R. H. & Clarke, D. B. (1976). Oxide and sulphide mineralogy of the Peuyuk kimberlite, Somerset Island, N.W.T., Canada. *Contributions to Mineralogy and Petrology* **56**, 157–172.
- Mitchell, R. H. & Letendre, J. (2003). Mineralogy and petrology of kimberlite from Wemindji, Quebec. In: *8th International Kimberlite Conference, Long Abstracts*. Elsevier, pp. 1–5.
- Mitchell, R. H. & Meyer, H. O. A. (1980). Mineralogy of micaceous kimberlite from the Jos Dyke, Somerset Island, N.W.T. *Canadian Mineralogist* **18**, 241–250.
- Mitchell, R. H. & Meyer, H. O. A. (1989). Mineralogy of micaceous kimberlites from the New Elands and Star Mines, Orange Free State, South Africa. In: Ross, J. & Jaques, A. L. (eds) *Proceedings of the 4th International Kimberlite Conference. Geological Society of Australia Special Publication*, **14**, 83–96.
- Mogg, T., Kopylova, M., Scott Smith, B. & Kirkley, M. (2003). Petrology of the Snap Lake Kimberlite, NWT, Canada. In: *8th International Kimberlite Conference, Extended Abstracts*. Victoria, BC, abstract 67.
- Naidoo, P., Stiefenhofer, J., Field, M. & Dobbe, R. (2004). Recent advances in the geology of Koffiefontein Mine, Free State Province, South Africa. In: Mitchell, R. H., Grutter, H. S., Heaman, L. M., Scott Smith, B. H. & Stachel, T. (eds) *8th International Kimberlite Conference Proceedings*. Amsterdam: Elsevier, pp. 161–182.
- Natland, J. H. (1989). Partial melting of a lithologically heterogeneous mantle: inferences from crystallization histories of magnesian abyssal tholeiites from the Siqueiros Fracture Zone. In: Sanders, A. D. & Norry, M. J. (eds) *Magmatism in the Ocean Basins. Geological Society, London, Special Publications* **42**, 41–70.
- Nielsen, T. F. D., Jebens, M., Jensen, S. M. & Secher, K. (2006). Archetypal kimberlite from the Maniitsoq region, southern West Greenland and analogy to South Africa. *Geological Survey of Denmark and Greenland Bulletin* **10**, 45–48.
- Nowicki, T., Crawford, B., Dyck, D., Carlson, J., McElroy, R., Oshust, P. & Helmstaedt, H. (2004). The geology of kimberlite pipes of the Ekati property, Northwest Territories, Canada. In: Mitchell, R. H., Grutter, H. S., Heaman, L. M., Scott Smith, B. H. & Stachel, T. (eds) *8th International Kimberlite Conference Proceedings, Vol. 1*. Amsterdam: Elsevier, pp. 1–27.
- O'Brien, H. E. & Tyni, M. (1999). Mineralogy and geochemistry of kimberlites and related rocks from Finland. In: Gurney, J. J., Gurney, J. L., Pascoe, M. D. & Richardson, S. H. (eds) *Proceedings of the 7th International Kimberlite Conference, Vol. 1*. Cape Town: University of Cape Town, pp. 625–636.
- Pasteris, J. D. (1980). Opaque oxide phases of the De Beers Pipe Kimberlite (Kimberley, South Africa) and their petrologic significance. Ph.D. thesis, Yale University, New Haven, CT, 463 pp.
- Poustovetov, A. (2000). Numerical modeling of chemical equilibria between chromian spinel, olivine and basaltic melt, with petrologic applications. Ph.D. thesis, Queen's University, Kingston, Ont. 136 pp.
- Price, S. E., Russell, J. K. & Kopylova, M. G. (2000). Primitive magma from the Jericho Pipe, N.W.T., Canada: Constraints on primary kimberlite melt chemistry. *Journal of Petrology* **41**(6), 789–808.
- Reid, A. M., Donaldson, C. H., Dawson, J. B., Brown, R. W. & Ridley, W. I. (1975). The Igwisi Hills extrusive 'kimberlites'. In: Ahrens, L. H., Dawson, J. B., Duncan, A. R. & Frank, A. J. (eds) *Physics and Chemistry of the Earth, 9*. Oxford: Pergamon Press, pp. 199–218.
- Rock, N. M. S. (1986). The nature and origin of ultramafic lamprophyres: Alnöites and allied rocks. *Journal of Petrology* **27**, 155–196.
- Roeder, P. L., Poustovetov, A. & Oskarsson, N. (2001). Growth forms and composition of chromian spinel in MORB magma: Diffusion-controlled crystallization of chromian spinel. *Canadian Mineralogist* **39**, 397–416.

- Roeder, P. L., Thornber, C., Poustovetov, A. & Grant, A. (2003). Morphology and composition of spinel in Pu'u 'O'o lava (1996–1998), Kilauea volcano, Hawaii. *Journal of Volcanology and Geothermal Research* **123**, 245–265.
- Roeder, P. L., Gofton, E. & Thornber, C. (2006). Cotectic proportions of olivine and spinel in olivine-tholeiitic basalt and evaluation of pre-eruptive processes. *Journal of Petrology* **47**(5), 883–900.
- Sack, R. O. & Ghiorso, M. S. (1991). Chromian spinels as petrogenetic indicators: Thermodynamics and petrological applications. *American Mineralogist* **76**, 827–847.
- Schulze, D. (2001). Origins of chromian and aluminous spinel macrocrysts from kimberlites in southern Africa. *Canadian Mineralogist* **39**, 361–376.
- Scott Smith, B. H. (1999). Near-surface emplacement of kimberlites by magmatic processes. *IAVCEI Commission on Explosive Volcanism Newsletter*, 3–11.
- Scott Smith, B. H., Orr, R. G., Robertshaw, P. & Avery, R. A. (1995). Geology of the Fort a la Corne Kimberlites, Saskatchewan. In: *Short Abstracts, 6th International Kimberlite Conference, Novosibirsk, Russia*. New York: Allerton Press, pp. 543–547.
- Shee, S. R. (1984). The oxide minerals of the Wesselton Mine kimberlite, Kimberley, South Africa. In: Kornprobst, J. (ed.) *Kimberlite I: Kimberlites and Related Rocks*. New York: Elsevier, pp. 59–73.
- Shee, S. R. (1985). The petrogenesis of the Wesselton Mine kimberlites, Kimberley, Cape Province, R.S.A. Ph.D. thesis, University of Cape Town.
- Smith, C. B. (1983). Pb, Sr and Nd isotopic evidence for sources of southern African Cretaceous kimberlites. *Nature* **304**, 51–54.
- Smith, C. B., McCallum, M. E., Coopersmith, H. G. & Eggler, D. H. (1979). Petrochemistry and structure of kimberlites in the Front Range and Laramie Range, Colorado–Wyoming. In: Boyd, F. R. & Myer, H. O. A. (eds) *Kimberlites, Diatremes and Diamonds: Their Geology, Petrology and Geochemistry*. Washington, D.C.: American Geophysical Union, pp. 178–189.
- Tappe, S., Foley, S. F., Jenner, G. A., Heaman, L. M., Kjarsgaard, B. A., Romer, R. L., Stracke, A., Joyce, N. & Hoefs, J. (2006). Genesis of ultramafic lamprophyres and carbonatites at Aillik Bay, Labrador: a consequence of incipient lithospheric thinning beneath the North Atlantic Craton. *Journal of Petrology* **47**(7), 1261–1315.
- Taylor, W. R. & Kingdom, L. (1999). Mineralogy of the Jagersfontein kimberlite—an unusual Group I micaceous kimberlite and a comment on the robustness of the mineralogical definition of 'orangeite'. In: Gurney, J. J., Gurney, J. L., Pascoe, M. D. & Richardson, S. H. (eds) *Proceedings of the 7th International Kimberlite Conference, Vol. 1*. Red Roof Design, Cape Town, pp. 861–866.
- Treiman, A. H. & Essene, E. J. (1984). A periclase–dolomite–calcite carbonatite from the Oka complex, Quebec, and its calculated volatile composition. *Contributions to Mineralogy and Petrology* **85**, 149–157.
- Ulrych, J., Pivec, E. & Rutsek, J. (1986). Spinel zonation in melilite rocks of the Ploucnice river region, Czechoslovakia. *Neues Jahrbuch für Mineralogie, Abhandlungen* **155**(2), 129–146.
- Van Rythoven, A. (2006). Petrology and geochemistry of kimberlite and mantle xenocrysts from Certac, Quebec. M.Sc. thesis, University of Toronto, Toronto, Ont.
- Van Straaten, B. I., Kopylova, M. G., Russell, J. K., Webb, K. J. & Scott Smith, B. H. (2006). Victor Northwest Kimberlite Pipe, Ontario: alternating volcanoclastic and apparent coherent extrusive rocks. *Kimberlite Emplacement Workshop Long Abstracts, Saskatoon, Saskatchewan, September 2006*.
- Whitlock, T. K. (1973). The Monastery mine kimberlite pipe. In: Nixon, P. H. (ed.) *Lesotho Kimberlites*. Maseru: Lesotho National Development Corporation, pp. 214–218.